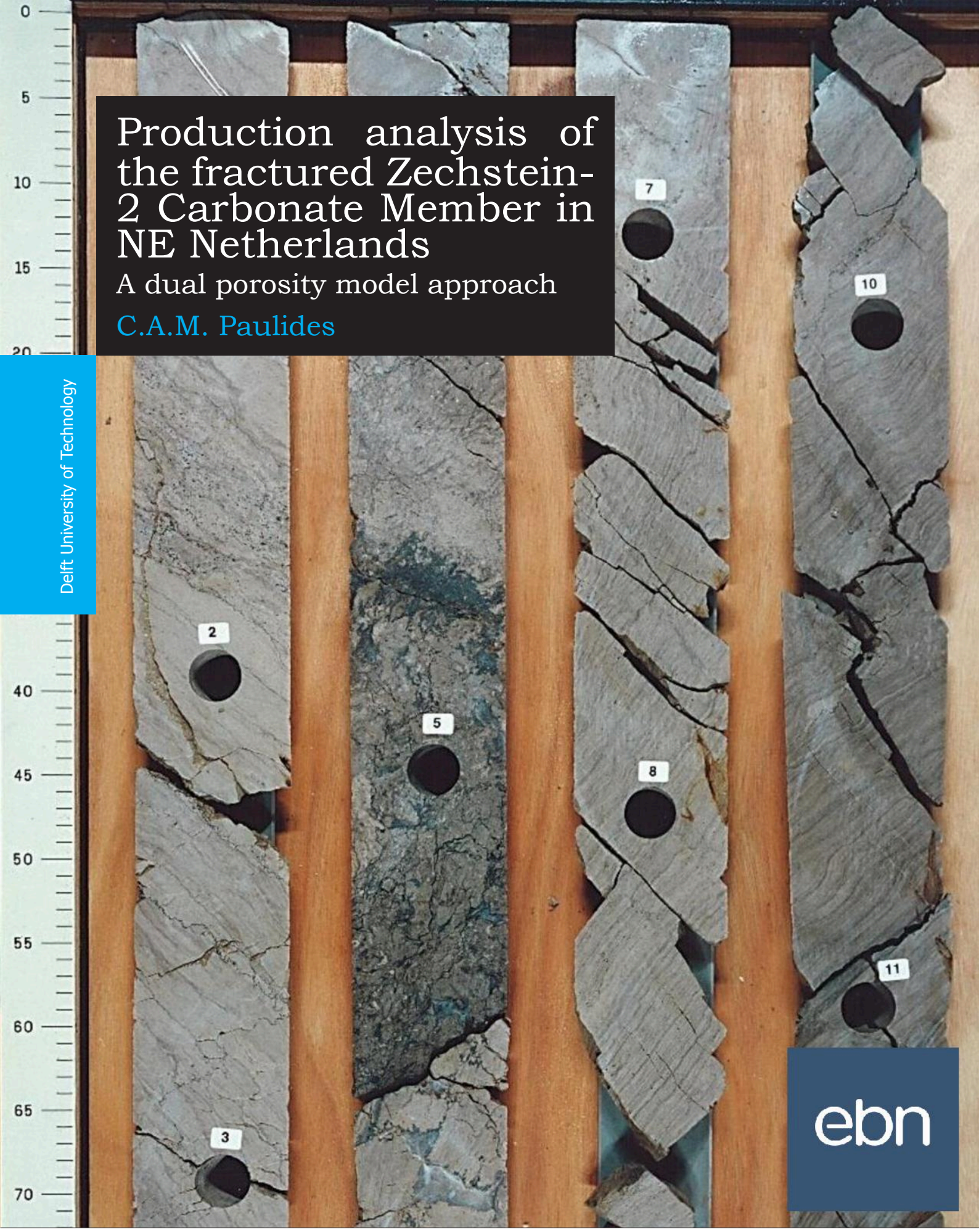

Production analysis of the fractured Zechstein-2 Carbonate Member in NE Netherlands

A dual porosity model approach

C.A.M. Paulides

Delft University of Technology

ebn

TU Delft Delft University of Technology

Challenge the future

Production analysis of the fractured Zechstein-2 Carbonate Member in NE Netherlands

A dual porosity model approach

by

C.A.M. Paulides

in partial fulfillment of the requirements for the degree of

Master of Science
in Petroleum Engineering

at the Delft University of Technology,
to be defended publicly on Friday July 8, 2016 at 11:00 AM.

Supervisor:	Prof. dr. G. Bertotti	
Thesis committee:	Dr. D. Voskov,	TU Delft
	Dr. N. J. Hardebol,	TU Delft
	Dr. Ir. R. R. G. G. Godderij,	EBN
	Ir. W. Eikelenboom,	EBN
	Drs. B. Jaarsma,	EBN

This thesis is confidential and cannot be made public until July 8, 2016.

TU Delft Delft University of Technology

Abstract

The Zechstein carbonates are an established petroleum play in North-West Europe including the Netherlands. Several undrilled Zechstein buildups have been identified around the Elbow Spit High in the northern part of the North Sea with GIIPs ranging from 1 to $10 \cdot 10^9\ m^3$. Since only few wells penetrate the Zechstein carbonates in this area, little information is known on productivity potential. Analogue studies of the Zechstein-2 Carbonate Member helps to understand the carbonate plays and increases the success rate of a potential drilling program. 20 gas fields in the Drenthe province in the Netherlands, with cumulative reserves of $57 \cdot 10^9\ m^3$, have been successfully producing from Late Permian Zechstein level for over more than 60 years. The objective of this study is to decrease the uncertainty of well and reservoir performance around the Elbow Spit High and other prospects through an analogue study of the Zechstein-2 Carbonate Member in the Drenthe province.

The Zechstein-2 Carbonate Member varies highly in production behavior. Generally, porosity increases from basin- towards platform-facies and consequently reservoir quality improves towards platform facies. Porosity in basinal and distal slope facies tend to be very low (0-5%) and fracture networks become a main controlling parameter on reservoir quality. Predicting these fracture networks is viable for a sustainable field development. Due to the distinction between matrix and fracture porosity, corresponding fluid storage and conductivity characteristics these reservoirs can be classified as dual porosity reservoirs. Typical naturally fractured reservoirs show two distinct decline rate periods with a constant flow period in between.

In this report, decline curve analysis from available production data is used to model the production decline and estimate reservoir parameters. The Warren & Root dual porosity model for constant pressure production is used to estimate the matrix-fracture storativity ratio, inter-porosity flow and reservoir size. Most Zechstein-2 Carbonate Member wells show a very high initial flow rate, fast decline and a moderate linear decline until the end of the lifetime. Platform facies reservoirs with high porosity are the best potential candidates for exploitation because of the high initial flow rates ($27.000\ \frac{m^3}{day}$ per meter of reservoir) and largest connected gas volumes ($9 \cdot 10^8\ m^3$). They do not show a direct correlation to the fracture networks although flow rates increase when placed nearby large open faults. Low porosity reservoirs (distal- to proximal slope facies) are highly dependent on the fracture network present. Initial flow rate per meter reservoir and cumulative gas production decreases to $3.500\ \frac{m^3}{day}$ per meter of reservoir and $2 \cdot 10^8 m^3$, respectively. These wells show an increase in initial flow rate and connected gas volumes with increasing distance to the nearest open fault.

The present-day principal stress in the Drenthe province is mainly parallel to the extensional open fracture trend and has probably contributed to their preservation. Consequently, knowledge on structural deformation history and present-day stress fields is compulsory for field development of low porosity carbonates. Wells should be drilled perpendicular to the maximum principle stress to encounter the highest open fracture density.

C.A.M. Paulides
Delft, July 2016

Acknowledgements

This research was written commissioned by the Delft University of Technology and supported by EBN. I would like to thank my supervisors Prof. Dr. G. Bertotti (TU Delft), Dr. Ir. R.R.G.G. Godderij (EBN), Ir. W. Eikelenboom (EBN) and Drs. B. Jaarsma (EBN) for their support, suggestions and feedback.

Further I would like to thank:

EBN for providing the data, facilitating and giving me the opportunity for writing my thesis on their behalf.

The NAM for providing the cores analyzed at the core store in Assen.

Delft University of Technology Department of Geosciences and Engineering for providing support and guidance.

Family, girlfriend and friends for their support throughout my study period.

Contents

1

Introduction

1.1. Zechstein Carbonates Revisited

Zechstein carbonates are an established petroleum play in North-West Europe including the Netherlands. A new Zechstein-2 Carbonate distribution and facies map for the Dutch northern offshore has resulted from thorough review of well and seismic data (Figure 1.1). Several undrilled Zechstein buildups have been identified with GIIPs ranging from 1 to $10 \cdot 10^9$ m^3 which could be combined with other targets.

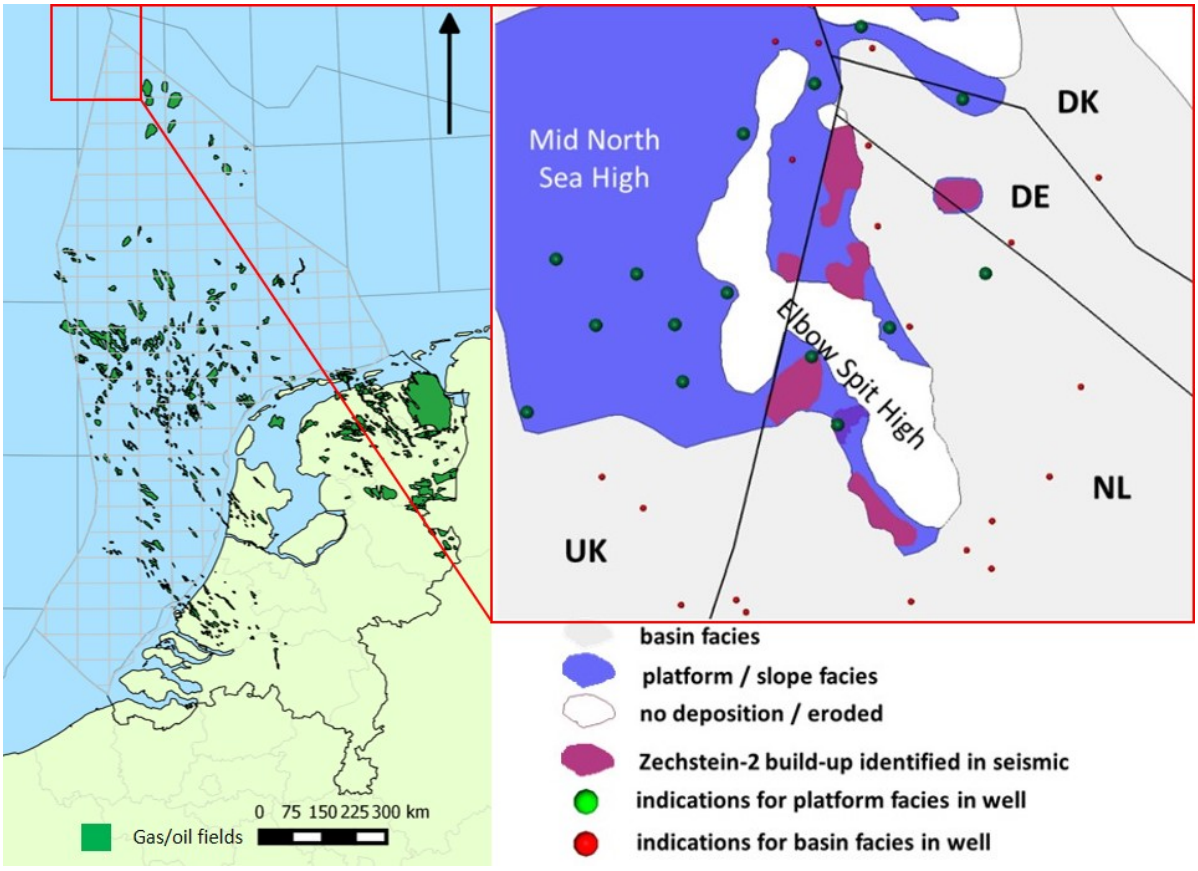

Figure 1.1: Present-day facies distribution map for Zechstein-2 carbonates around the Elbow Spit High. [1] [2] [3]

Since most parts of the prospects around the Elbow Spit High are undrilled, little information is known on the productivity potential. Analogue studies of the Zechstein-2 Carbonate Member helps to

understand the carbonate plays and increases the success rate of a potential drilling program. The aim of this study is to reduce the uncertainty on reservoir productivity and provide a detailed description on the different parameters controlling productivity in carbonate reservoirs. The north-eastern part of the Netherlands (NEN) is used as an analogue for the Elbow Spit High (ESH) (Figure 1.2) because of its comparable platform-to-basin profile and of its successful and extensive exploitation history of carbonate hydrocarbons. It has been an outstanding hydrocarbon province since the late 1950's. A strong oil smell from cores of the basal Zechstein carbonates and Carboniferous sandstones (Corle-1) extracted in 1923 increased the interest in potential prospective reservoirs in this area. In 1948, the first gas well (Coevorden-1) in the Netherlands successfully started production at Late Permian Zechstein level. After this discovery, multiple wells have been drilled which eventually led to the discovery of the giant Groningen gas field in 1959, which changed the Dutch gas market considerably. Ever since the Coevorden-1 well, the Nederlandse Aardolie Maatschappij (NAM) has actively explored the potential of the Zechstein-2 Carbonate play in the south-east of Drenthe province and has resulted in a total of 20 producing gas fields with cumulative reserves of $57 \cdot 10^9\ m^3$ in the Zechstein-2 Carbonate (ZEZ2C) Member. [4]

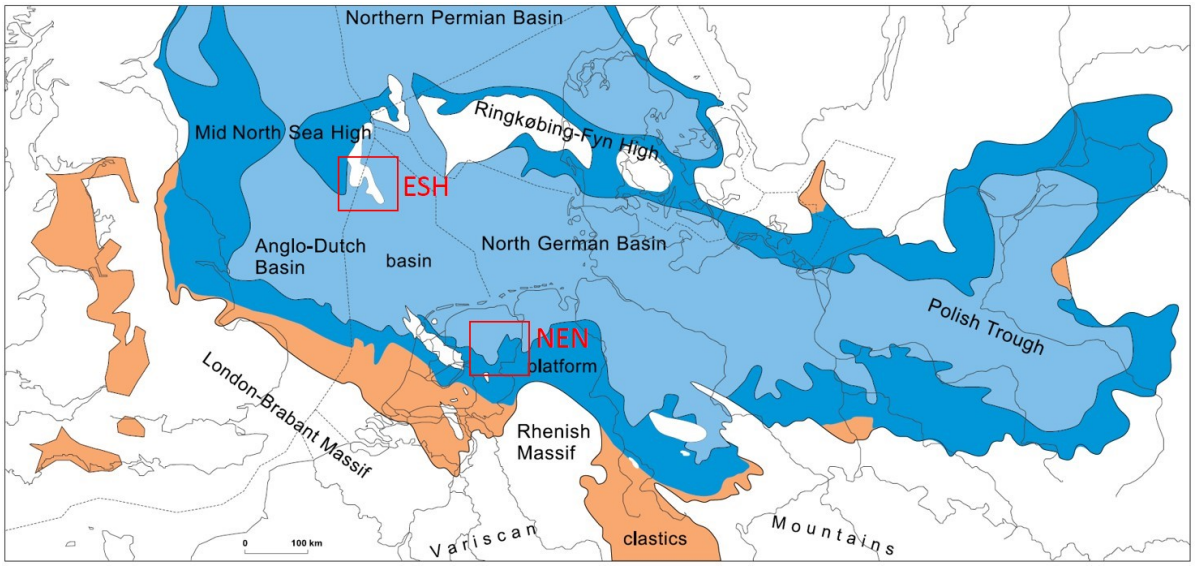

Figure 1.2: Map showing the extent of the Zechstein evaporitic basin in the Late Permian time. [5] ESH: Elbow Spit High. NEN: North-East Netherlands. NEN is used as an analogue study for the ESH because of its successful and extensive exploitation history of hydrocarbons of the Zechstein-2 Carbonate Member.

1.2. Study objectives

The objective of this study is to decrease the uncertainty of well and reservoir performance around the Elbow Spit High and other prospects through an analogue study of the Zechstein-2 Carbonate Member in North-East Netherlands. Increased knowledge of the main parameters that control reservoir quality will lead to an enhanced rate of success for future prospect drilling programs. Estimate and elucidate reservoir parameters which are visible on seismic maps (e.g. faults, fracture networks, basin-platform relief, etc.) influencing reservoir quality are therefore the main targets of this study. Reservoir parameters are estimated by a decline curve study based on a dual porosity model. The study objectives are as follows:

- To understand the geology of the Zechstein Group
- To understand the structural deformation of the area of interest
- To understand and predict the key parameters controlling reservoir quality
- To raise interest for future developments around the Elbow Spit High and other carbonate prospects

1.3. Area of interest

The area of interest for this study is located in the south-eastern part of Drenthe covering an area of approximately $25.000\ m^2$. Its borders are defined by the cities of Coevorden on the west, Emmen on the north and the German border at the eastern and southern boundaries. A total of 20 fields have been developed in this area producing mainly from three distinct levels; the Zechstein-2 Carbonate Member, Carboniferous sandstones and the Rotliegend sandstones. The wells should satisfy four primary selection criteria for this analysis:

1. Wells produce merely from the Zechstein-2 Carbonate Member
2. Wells fully penetrate the 'Basal Zechstein Unit'
3. Availability of sufficient data to construct reasonable production profiles
4. Extra well data includes well-test data or core measurements

23 wells meet these criteria and cover a total of 7 different gas fields in South-East Drenthe area (Figure 1.3). The assets belong to the Schoonebeek and Drenthe IIb consessions which are operated by the NAM. Generally, the Zechstein-2 Carbonate Member consists of poor quality basinal reservoir rocks with increasing productivity towards the more porous and permeable proximal slope and platform. Several techniques have been applied by the NAM to improve the productivity and connectivity of the reservoirs, including horizontal drilling, short radius sidetracks, multi-lateral holes, under-balanced coil-tubing drilling, hydraulic fracturing and acid stimulation

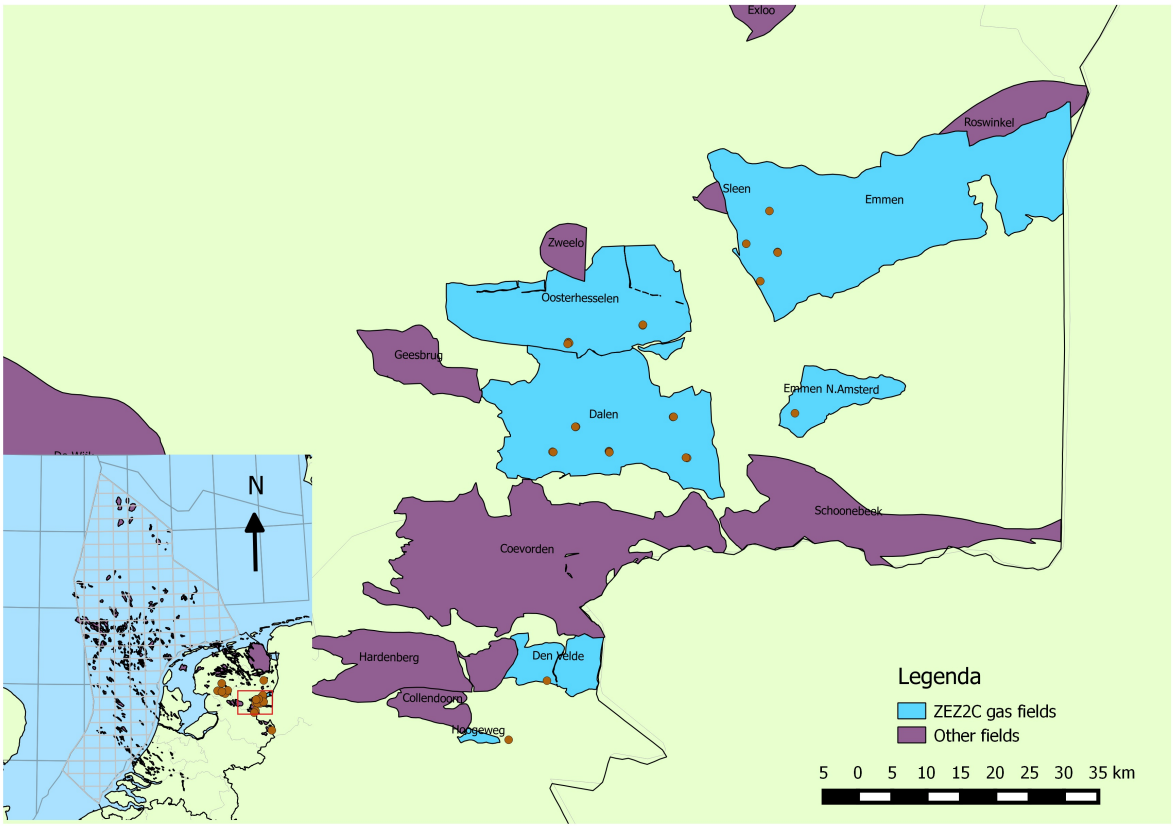

Figure 1.3: Map of SE Drenthe showing Zechstein-2 Carbonate Member gas fields used in this study (blue) and other producing gas fields in the area (purple). Dots represent surface location of the wells. Note that often multiple wells depart from a single surface location.

1.4. Naturally fractured carbonate reservoir modeling

Rate transient analysis is the best method for analyzing the initial performance of a well. But rate transient analysis is not always available for many wells and certainly not over the whole life-time of a

well, especially for very old wells producing from the Zechstein-2 Carbonate Member in Drenthe. If rate transient data is not available, then decline curve analysis from available production data can be used to model the production decline and to estimate reservoir parameters. Several authors have developed decline curve theories, mostly for homogeneous (conventional) reservoirs. Arps developed the emperical standard exponential, hyperbolic and harmonic decline equations [6]. Fetkovich constructed log-log type curves, combining all equations developed by Arps with the analytical constant pressure solutions of slightly compressible fluids. These two methods are highly simplified, assuming constant bottom-hole pressure and neglect variations in fluid properties. Many other authors such as Carter, Palacio, Blasingame and Anash followed the work of Arps and Fetkovich and developed enhanced methods for decline curve analysis. Nevertheless, all models describe homogeneous (conventional) reservoirs and were not developed to describe naturally fractured reservoirs. The studies of Da Prat and Hebert improved naturally fractured reservoir modeling and found solutions for infinite and finite acting naturally fractured reservoirs for the Warren & Root fracture model. Da Prat found that a typical naturally fractured reservoir decline (using constant bottom-hole pressure) had two distinct decline rate periods with a constant flow rate period in between. Few studies have been done on modeling naturally fractured reservoirs and existing decline curve analysis for homogeneous reservoirs is not always applicable.

Limitations of decline curve analysis of naturally fractured reservoirs It is often impossible to analyze production data of naturally fractured reservoirs due to multiple reasons [6]:

- Decline models of naturally fractured reservoirs do not consider variations of fluid properties with pressure changes of well bottom-hole pressure with time.
- Some naturally fractured reservoirs show similar production trends as homogeneous (conventional) reservoirs

1.5. Document structure

The structure of the report is briefly explained in the following paragraph. The geological history and structural deformation of the Zechstein-2 Carbonate and the 'Basal Zechstein Unit' are described in chapter 2. The facies present in the Zechstein-2 Carbonate Member are separately addressed and their characteristics will be discussed in the paragraphs of this chapter. Chapter 3 explains the theory, model and input parameters which are used to predict the production profiles. The results are described in chapter 4 outlining the main parameters which control reservoir quality. Chapter 5 and 6 include discussion and conclusion reviewing the quality, validity and methodology used for this study. The core fracture analysis is a parallel study to support the chosen parameters for the model and is also discussed in chapter 5. In chapter 7 recommendations are given for future studies.

2

Zechstein-2 Carbonate Member

The Zechstein-2 Carbonate Member is part of the larger Upper Permian Zechstein Group and contains important hydrocarbon reservoirs. The Zechstein-2 Carbonate Member consists of poor quality basinal reservoir rocks and increasing productivity towards the more porous and permeable proximal slope and platform and is therefore one of the main parameters controlling reservoir quality. The Zechstein-2 Carbonate Member in the area of interest comprises of an East-West trending carbonate platform [7] with basinal facies northwards and lagoonal facies southwards of this trend (Figure 2.5). The slope in between consists of proximal slope facies nearby the platform edge and distal slope facies far away from the platform edge into the basin. The depositional environment of these different facies was mainly controlled by basin tectonics and cyclic variation in paleobathymetry. This section explains the cyclic deposition of the main members of the Upper Permian Zechstein Group.

2.1. Geology of the Zechstein Group

2.1.1. The Southern Permian Basin

Carbonate and evaporites precipitate through various abiological and biological mechanisms. The Zechstein Group contains both of these mechanisms in abiological evaporite precipitation (e.g. Zechstein-1 Anhydrite Member) and mainly biological precipitated carbonates (e.g. Zechstein-2 Carbonate Member). The cyclic interaction between these mechanisms and associated diagenetic processes leads to a large variety in depositional facies. The Upper Permian Zechstein Group consists of five cyclic depositional sequences of carbonate and evaporitic rock (Figure 2.1). These sequences are locally preceded by thin clastic deposits and are further characterized by a succession of carbonate, anhydrite and halite deposits.

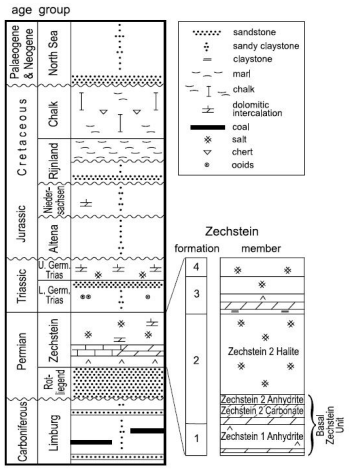

Figure 2.1: Generalized stratigraphy of the NE Netherlands with details of the Zechstein Group.[8]

The lower members of the Zechstein Group constitute of non-mobile rock units formed prior to the deposition of the first thick and ductile Zechstein salt, namely the Zechstein-2 Halite Member. Distinction is made between the non-mobile lower members and the upper ductile members. These non-mobile lower members are informally known as the 'Basal Zechstein Unit' (Figure 2.1). The Zechstein Group overlies the Lower Permian Rotliegend Group and was deposited during the Late Permian transgression of the intra-continental Zechstein sea which flooded the European Permian basins. The Zechstein sea was located at a latitude of approximately 10° in an arid climate which led to the cyclic evaporate depositions (Figure 2.1). Five Zechstein cycles have been identified in the Dutch subsurface. The three lower cycles (Zechstein-1,-2 and -3) developed under normal marine conditions and the clastic influx was restrained to the basin margins. During the two upper cycles hypersaline conditions prevailed and no carbonates were deposited.The thickness of the total Zechstein Group extends from over 1200 m in the northern offshore to less than 50 m in the southern Netherlands [1].

2.1.2. Zechstein-1 Formation

The base of the Zechstein Group is marked by a basin wide occurrence of an one-meter-thick layer of shales (the Coppershale). This was the first deposit after the transgression which flooded the whole Southern Permian Basin. Before increasing salinity led to the precipitation of sulphate, a thin carbonate unit was deposited. The carbonate platform facies of the Zechstein-1 accumulated in an East-West trending direction in the middle part of the Netherlands with slopes dipping northwards (Figure 2.2). Due to the hot and arid climate, evaporation rates were high and rapid gypsum accumulation occurred in shallow-water areas building up towards sea-level. Due to sulphate reducing bacteria concentrated at chemocline level, the gypsum was effectively consumed resulting in little or no gypsum accumulation at greater depths than approximately 15 meter (Figure 2.3). The variation in gypsum accumulation between basin and shallow water resulted in a distinct basin relief where the platform of the Zechstein-1 Anhydrite Member eventually stood 250-300 m higher than the adjacent starved basin. [7]

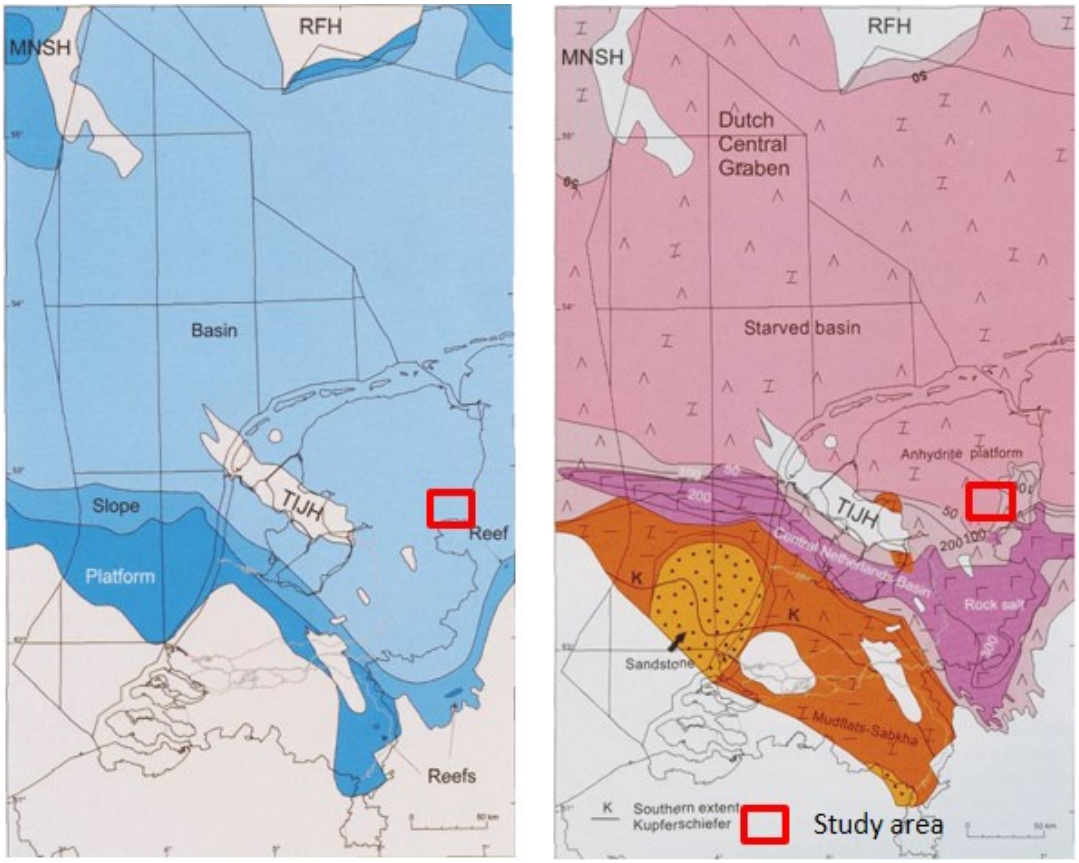

Figure 2.2: Facies map of the ZEZ1 Carbonate Member with carbonate platforms in the southern part of the Netherlands (left). Facies and isopach map of the ZEZ1 Anhydrite Member (right).[4]

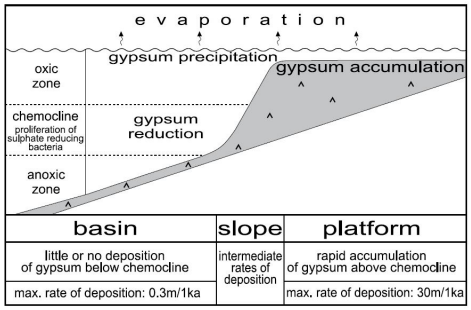

Figure 2.3: Principles of the suplhate platform development of the Zechstein 1 Anhydrite Member in the NE Netherlands. [7]

2.1.3. Zechstein-2 Formation

A subsequent rise of sea level resulted in a decrease of salinity and effectively changed the sedimentation from gypsum to carbonates. The carbonate facies show a North-South trending basin-to-platform profile. As this transgression was not as extensive as the previous transgression, the depositional profile does not coincide with those of the Zechstein-1 nor the Zechstein-3 Carbonate Members (figure 2.4). As a result of sea level fall, salinity increased and carbonate deposition was replaced by gypsum precipitation. This led to the accumulation of the Zechstein-2 Anhydrite Member with the thickest accumulations in the shallow waters of the upper slope and platform deposits. A continuing sea level fall resulted in a change in the nature of evaporate precipitation from gypsum to halite. Because the sea level had dropped below platform level, halite precipitation was mainly restricted to the basin and slope areas. This accumulation continued until the basin almost entirely filled the relief formed by the preceding members. As a result, the following members of the Zechstein Group do not show such a variation in relief but a rather featureless occurrence (figure 2.6).[4]

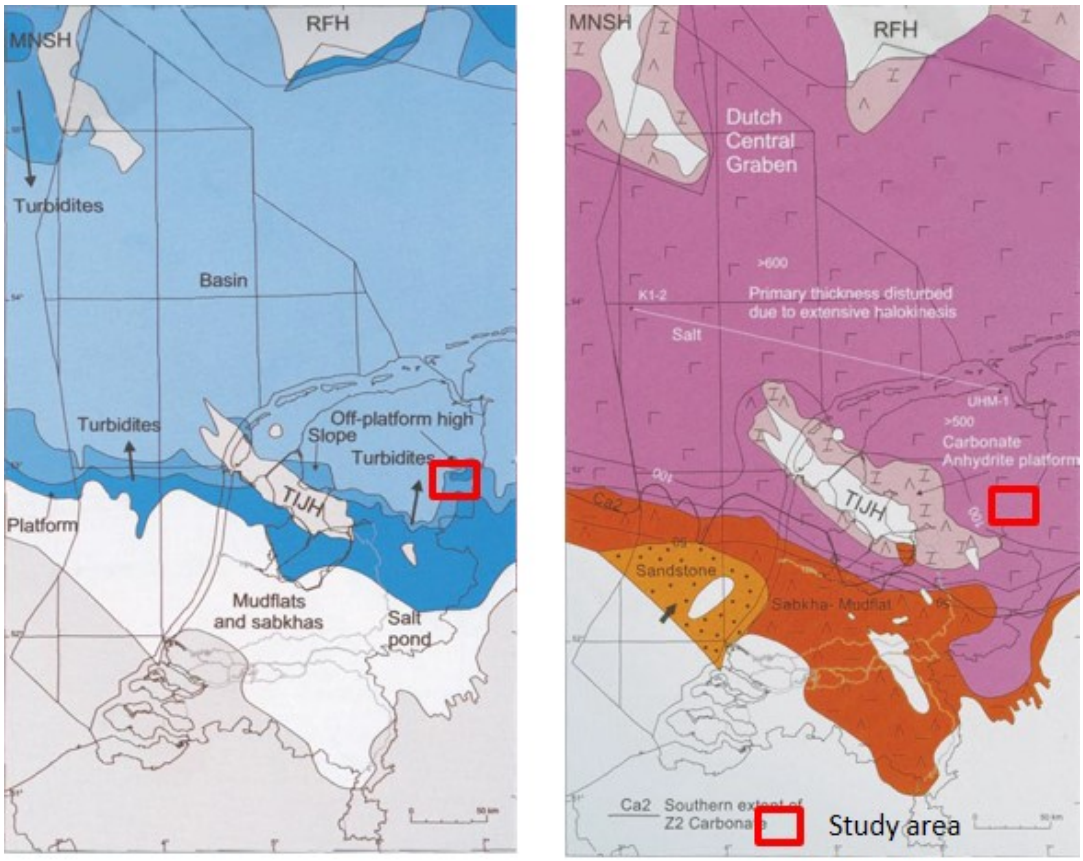

Figure 2.4: Facies map of the ZEZ2 Carbonate Member (left) and facies and isopach map of the ZEZ2 Anhydrite and Halite Member combined (right).[4]

2.2. Depositional model of the Zechstein-2 Carbonate Member

A logical classification with respect to these variations is important for porosity trend modeling in the Zechstein-2 Carbonate Member. This section contains an explanation of the main features of each depositional group accompanied by core photographs.[4] The facies of the Zechstein-2 Carbonate Member can be roughly subdivided into five main groups;

- Basinal facies
- Distal slope facies
- Proximal slope facies
- Shelf facies (i.e. oolite shoal)
- Lagoonal facies

All these facies can be found in the area of interest, which lies at the fringe of the platform and covers all interesting depositional facies (figure 2.5) [4]. The type of facies relates to the relief created by the Zechstein-1 Formation as shown in figure 2.6. Lagoonal facies represent very poor reservoirs and no wells were drilled into the lagoonal facies in this area. Therefore, this facies is not considered further in this analysis.

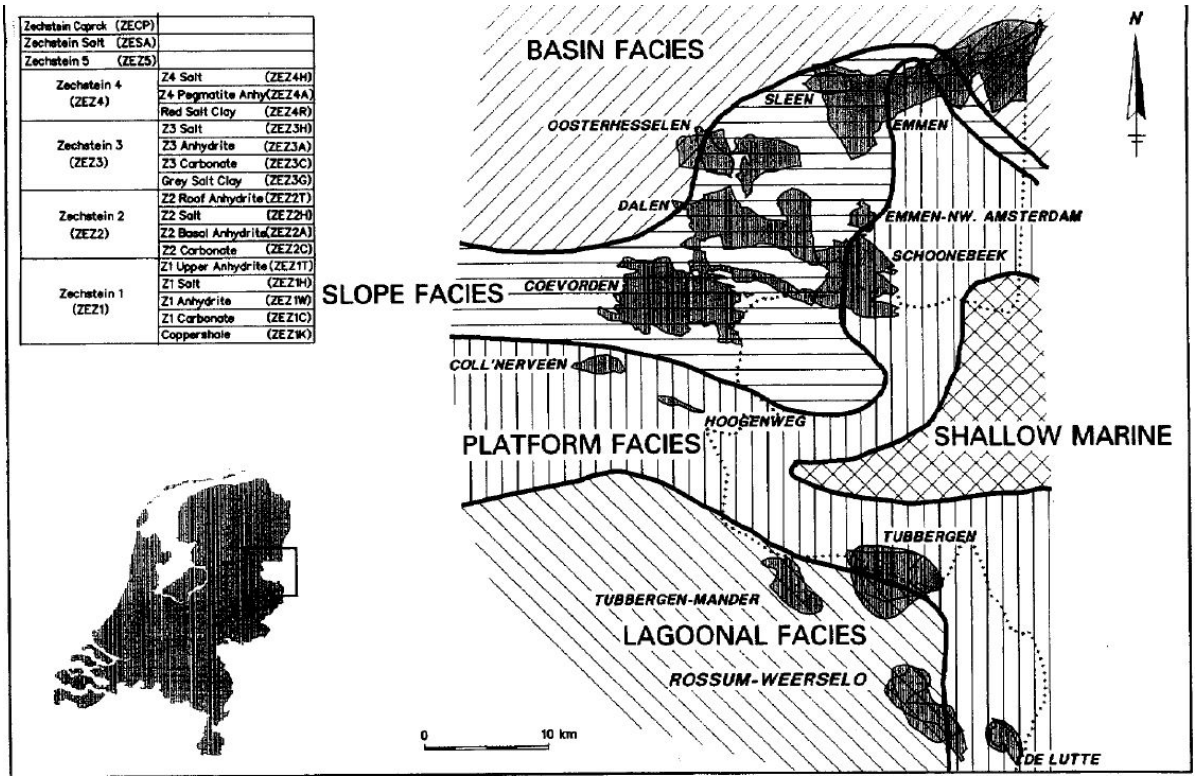

Figure 2.5: Facies distribution map of the ZEZ2C in SE Drenthe.[9]

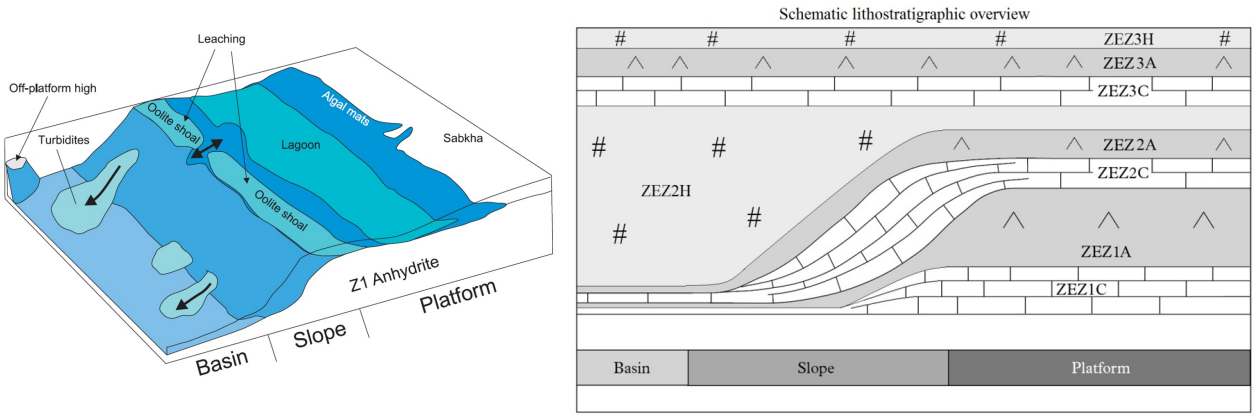

Figure 2.6: A simplified 3D depositional model of the Zechstein-2 Carbonate Member (left). 2D Model of deposition of the Zechstein-2 Anhydrite and the Zechstein-2 Halite Member that overlies the 'Basal Zechstein Unit' (right). [4]

2.2.1. Basinal facies

Basinal facies consist of interbedded evenly laminated lithology (hemipelagic) and turbidites.The hemipelagite consists of alternating light and dark laminae mostly 1-3 mm thick (figure 2.7). These facies are deposited at depths below the influence of storm-generated waves in an anoxic environment and generally have a thickness of 0-50 m. Nearby the carbonate platforms, displaced shelf deposits occur as slumps within these facies. Generally, porosity ranges from 0 to 2%. (figure 2.7) [4]

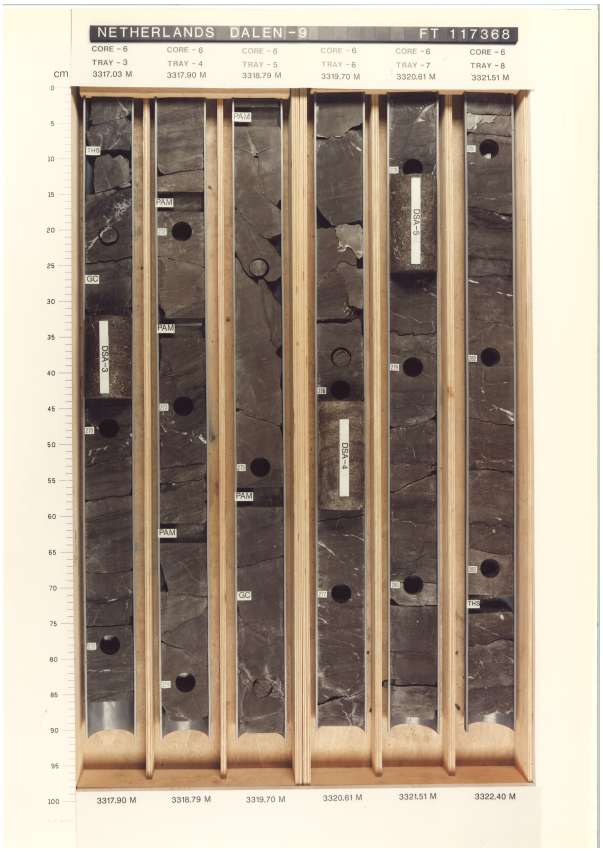

Figure 2.7: Core photograph of basinal facies in DALEN-09-S2 well. (www.nlog.nl)

2.2.2. Distal slope facies

Distal slope facies consist of light-coloured limestones, dolomites and occasional redeposited shelf sediments displaced by slumping and sliding. In the area of interest, the slope facies can reach a thickness of up to 150 m. The slope facies are an interplay between autochtonous grey mm-laminated dolomitised mudstones and allochtonous sediments originating from the proximal slope and shelf. Anhydrite is locally present in laminae, veins or nodules. Distinction can be made between graded bedding from turbidite flows and brecciated, highly fractured intervals from debris flows. The conglomeratic debris flows have considerable matrix porosity and permeability thus are potentially adequate reservoirs. Generally, porosity ranges from 0 to 5%. (figure 2.8; left) [4]

2.2.3. Proximal slope facies

Proximal slope facies consist of limestones and dolomitised mudstones. Proximal slope commonly show major slumping and sliding of sediments originating from the shelf. The redeposited sediments from the shelf mainly consists of ooids- and pisoids. Dolomitisation originates from leaching of meteoric waters into the temporarily exposed slope and platform during relative low sea level. Proximal slope facies occasionally show very high secondary vuggy porosity due to the leaching process, resulting in

good reservoir properties. Porosity ranges between 1 and 10%. (figure 2.8; right) [4]

2.2.4. Shelf facies

Shelf facies consist of a complex of oolitic, pelletoidal, bioclastic and pisolitic grainstones. Sediment deposition occurred in shallow water and was subjected to the same leaching processes during subaerial exposure as the proximal slope facies. Shelf facies tend to have high porosity and can reach values up to 20% (figure 2.9). [7] [4]

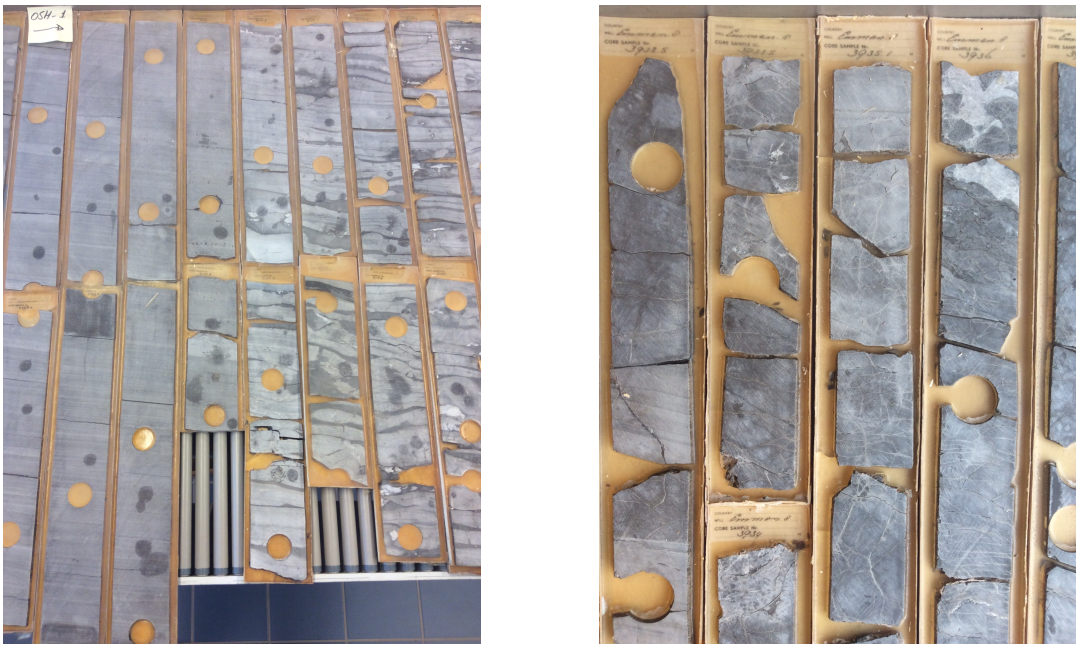

Figure 2.8: Core photograph of basinal facies in OOSTERHESSELEN-01 well (left) (picture taken at: NAM, Core Store Assen), Core photograph of proximal slope facies in EMMEN-08 well (right) (picture taken at: NAM, Core Store Assen).

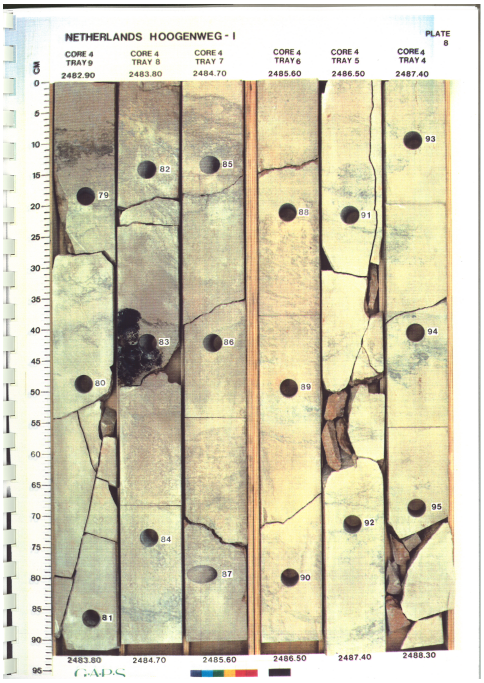

Figure 2.9: Core photograph of shelf facies in HOOGENWEG-01 (www.nlog.nl)

2.3. Structural deformation history of the NE Netherlands

The fault zones in the area of interest show signatures of dextral wrenching along deep-seated basement faults relating to a NNW-SSE oriented compression, originating from the Carboniferous Variscan orogeny. [5] As can be seen on the dip-map of the top Zechstein-2 Carbonate Member, given in figure 2.12 and appendix A.1, fault zones, including the Hantum fault zone and the West Groningen fault zone, show signatures of dextral wrenching. The NNW-SSE oriented fault patterns along the Lauwerszee Trough represent left-stepping synthetic Riedel shear fractures. These deformation patterns are characteristic for dextral wrenching and form in combination with other features such as antithetic Riedel faults, reverse faults, folds and extensional faults (figure A.1). The ENE-WSW trending faults within the Lauwerszee Trough are interpreted to represent the antithetic Riedels. These antithetic Riedels, as well as the synthetic Riedels, exhibit significant strike-slip components (up to 750 m) besides significant dip-slip components (up to 400 m). [9] The wrench fault systems of the Lauwerszee Trough branch to the north-west and are probably linked to the younger fault systems bounding the Central Graben. These branch patterns are characterized by rhomboidal fault patterns e.g. the Anjum area and the Coevorden-Dalen-Oosterhesselen area in between the Holsloot and Coevorden wrench fault zones. [9]

Early Kimmerian deformation phases (end-Trias until begin-Jura) resulted in sinistral wrenching of the major wrench faults. As a result of the sinistral wrenching of the Holsloot fault zone, both Emmen and Schoonebeek have undergone dextral wrenching near-perpendicular to the major Holsloot wrench fault, characterized by the presence of left-stepping Riedels (Figure **??**). The presence of flower structures at various stratigraphic levels in the North-East Netherlands indicates that wrenching continued through time (Figure 2.10). The Late Kimmerian, Laramide and Late Alpine orogenic phases resulted in N-S to NNW-SSE compression and reactivation of the dextral wrench tectonics in the North-East Netherlands. [9]

The orientation of the major wrench tectonic compressive stresses can, in addition to expressions on dip-maps, best be deduced from the orientation of pop-up blocks, bounded by reverse faults. Such features develop perpendicular to the horizontal maximum principle stress. Several significant reverse faults are present in South-East Drenthe area and their orientation is largely East-West, indicating an overall North-South oriented maximum principal stress. At the end of the Carboniferous such (syn-sedimentary) reverse faults probably generated palaeo-highs on which the Zechstein-2 Carbonate Member platform developed. [9]

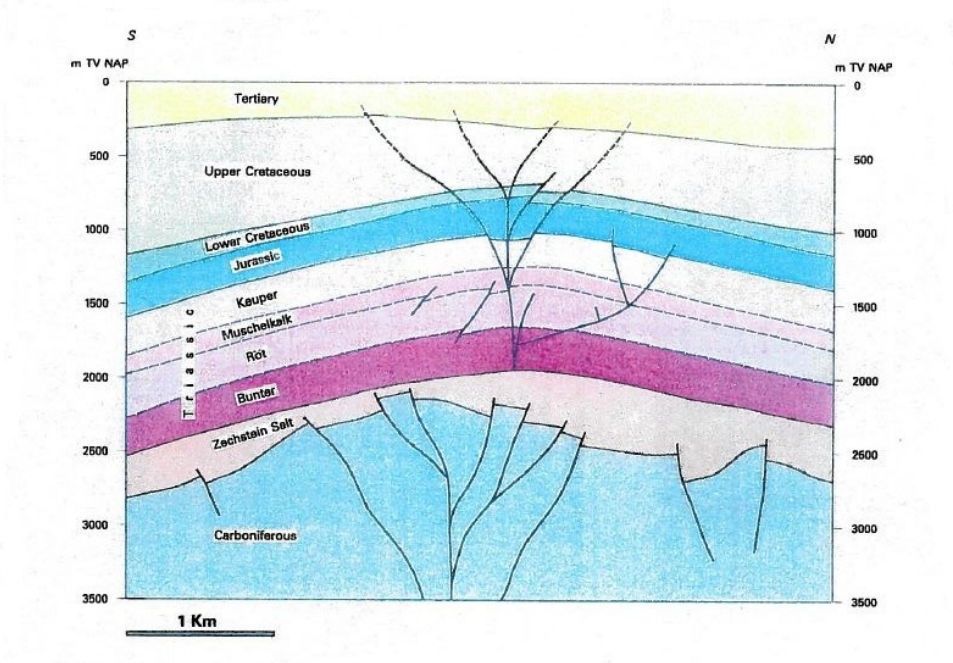

Figure 2.10: North-south structural cross-section of the Emmen area showing flower structures and reverse faulting/ pop-ups at Carboniferous level and at shallower levels, indicative of continued wrenching tectonics through time. [9]

2.3.1. Present-day stress field

The present-day horizontal maximum principal stress in the North-East Netherlands, as indicated by borehole breakouts from several Borehole Imaging Logs, ranges between NW-SE and N-S, dependent on the local stress regime of individual blocks. Previous studies by Frikken et al. show rose diagrams of fracture strike orientations of all Zechstein-2 Carbonate Member cores with three distinct fracture sets of which the orientation coincide with the described wrench tectonics. The open fracture sets relate to the extensional fractures and antithetic Riedel shear fractures. This orientation is also evident from hydraulic fracture stimulation of Rotliegend reservoirs. The present-day maximum principal stress is largely parallel to the extensional open fracture trend and has probably contributed to their preservation. These open fractures are extremely important for the enhancement of fluid flow and reservoir quality. [9]

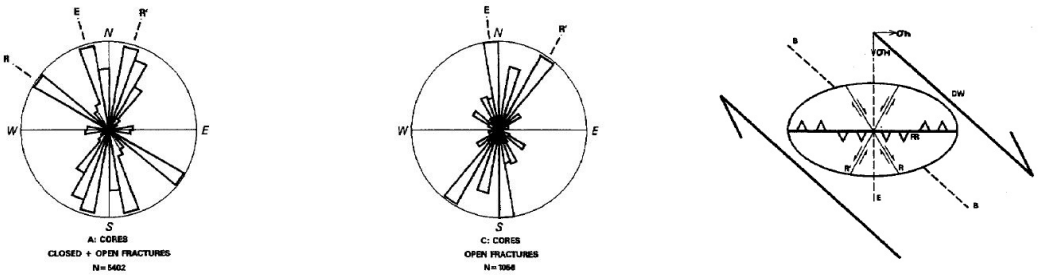

Figure 2.11: Rose diagrams of fracture strike orientations from all ZEZ2C cores in the South-East Drenthe area. The fractures show three distinct populations of which the orientations coincide with the described wrench tectonics. The open fractures sets relate to extensional fractures and antithetic Riedel shear fractures. [9]

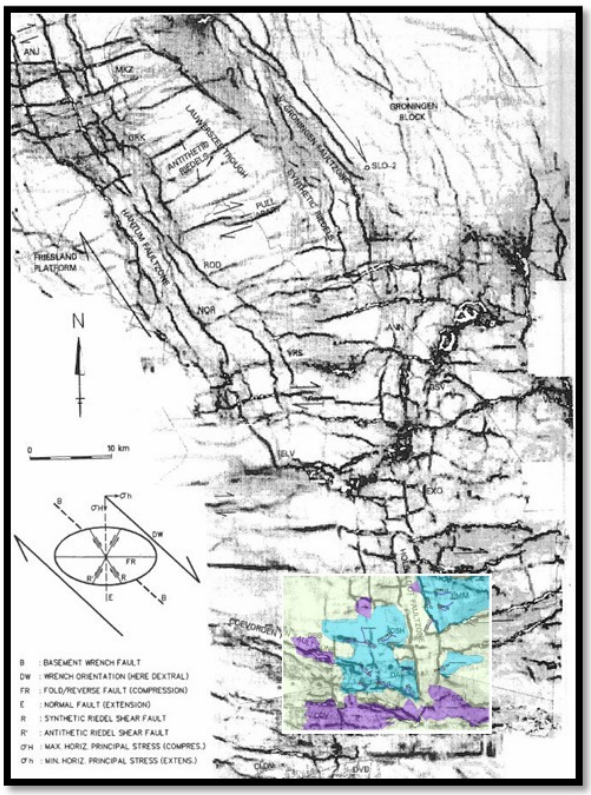

Figure 2.12: Dip-map of top Zechstein-2 Carbonate Member. En-echelon left-stepping Riedel faults, pull-apart basins and rhomboidal fault patterns are characteristic features of dextral wrenching. [9]

3

Method

Naturally fractured carbonate reservoirs exhibit a substantial variation in matrix and fracture permeability. Therefore, it has a large variation in terms of flow rate, decline and cumulative gas production. A good reservoir model will allocate the required parameters to predict the output parameter in a logical and consistent manner. Main parameters affecting the reservoir quality are porosity and permeability. Naturally fractured reservoirs are characterized by the presence of two distinct types of porous media: matrix and fracture (i.e. a dual porosity system). The dual porosity classification is derived from the differences in fluid storage capacities and conductivity characteristics for the two distinct types of porous media. Dual porosity systems often consists of an irregular system of vugs and natural fractures. Due to limiting reservoir simulation techniques these systems need simplification in a more regular and systematic model. Over the past few decades, several models have been proposed to represent the dynamic behavior in naturally fractured reservoirs. The main conceptual difference between these models is how fluid flow is described in the matrix. Most models assume that the fluid flows from matrix to the fracture system and subsequently into the wellbore (i.e. the matrix does not produce directly into the wellbore) (figure 3.1). The models also assume that the matrix storativity is considerably larger than fracture storativity and matrix permeability is considerably lower than fracture permeability. [10] The solutions for the flow rates are based on a model presented by Warren & Root (1963). Production analysis of the Zechstein-2 Carbonate Member can be modeled with two main input models (1 & 2) resulting in the production model (3) (figure 3.2);

1. A depositional model (including matrix porosity-permeability trends, thickness relationships, etc.).
2. A fracture network model (including fracture density, fracture aperture, fracture conductivity, etc.).
3. A production model (including initial flow rate, reservoir size, decline rate, etc.).

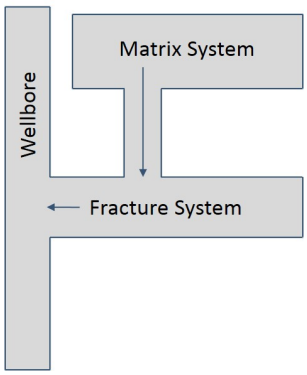

Figure 3.1: Flow scheme of a dual porosity system

First, the concept of the production model will be explained and subsequently the two input models (i.e. depositional model and fracture network model).

3.1. Workflow

The high level work flow is depicted below in figure 3.2.

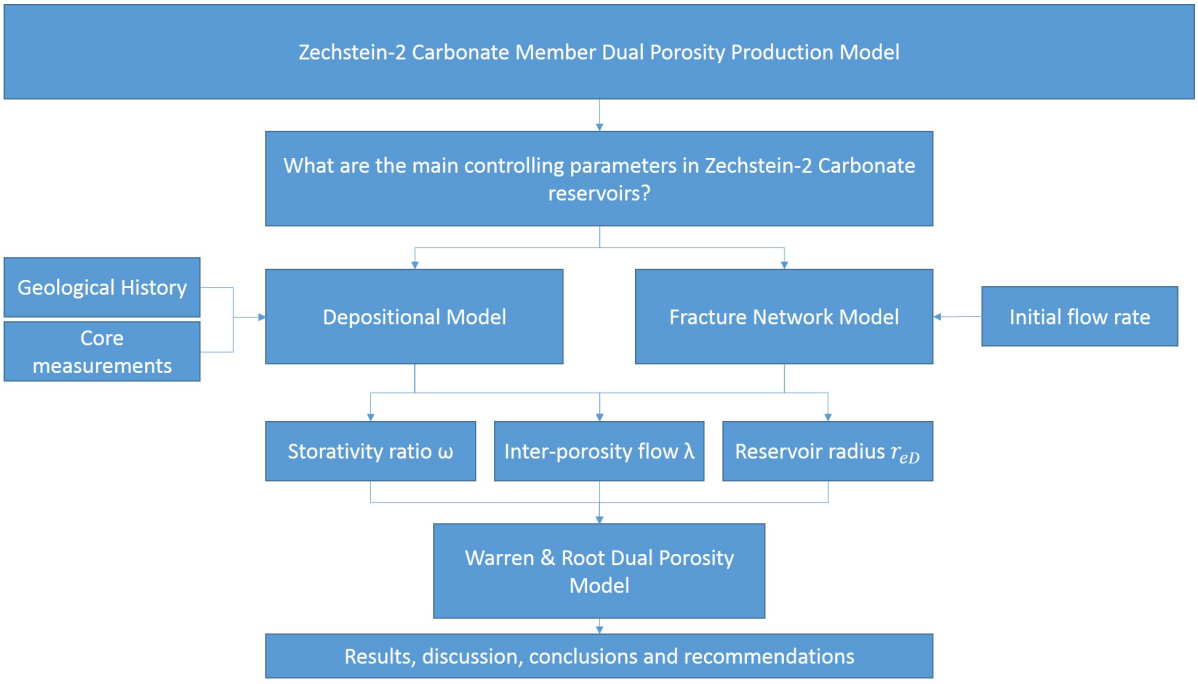

Figure 3.2: High-level workflow to obtain input parameters for the Warren & Root dual porosity model.

3.2. Data

Production data from the Zechstein-2 Carbonate Member is scarce and of very bad quality. 23 wells have monthly production data available while two of them have additional daily production data. A well is given as an example in figure 3.3. Important production information is lost when monthly data is used (e.g. initial high flow rates, flow rate shift from fracture-flow to matrix-flow). During the production lifetime of a well, the pressure difference between reservoir and bottom-hole is periodically increased to enhance flow. This results in a production profile of which the flow rate fluctuates in time. The model assumes a system of constant pressure production. Linking the model and real-time data, the superposition principle is assumed to state that the system reacts linear to pressure changes and that the total system output gives the same output as the sum of all separate constant pressure production periods as explained below:

Superposition Principle The superposition principle states that, for all linear systems, the net response at a given place and time caused by two or more stimuli is the sum of the responses which would have been caused by each stimulus individually. Thus, if input A produces response X and input B produces response Y then input (A + B) produces response (X + Y). [11] This means that the data can be sorted in descending order of flow rate to obtain a smoothed production profile.

When flow rates exceed facility capacity, the wells are choked to decrease flow rate. Due to this manual decrease in flow rate (figure 3.3), flow rates are affected and do not represent reservoir characteristics. This affects the resulting profile and therefore caution should be taken not to link reservoir properties to manually induced artifacts.

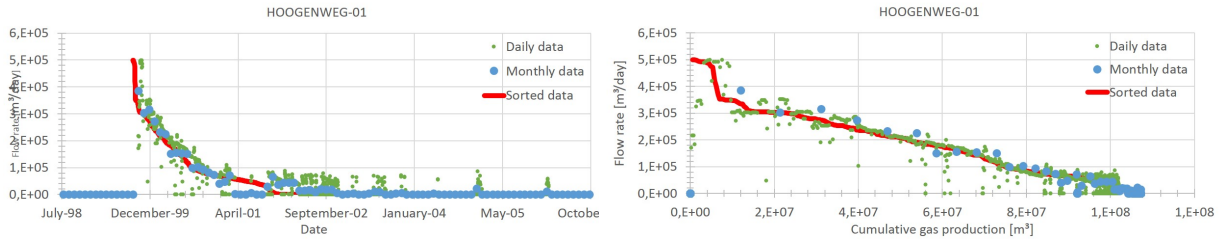

Figure 3.3: Production profile over time (left). Cumulative production profile (right).

3.2.1. Assumptions

Due to the real-life complications as explained above, some assumptions have to be taken into account to predict the systems behavior according to a dual-porosity model;

- The reservoir is only productive over the perforated interval and only horizontal flow into the wellbore occurs. This means that the productivity of one meter of vertical reservoir is calculated by total flow rate divided by the perforated interval.
- The initial flow rate is exclusively a product of fracture permeability.
- When the system is choked, an initial flow rate is assumed according to a best-fit decline curve (see best fits in appendix B.1).
- Perforated interval equals netto gas column.

3.3. Warren & Root dual porosity model

Naturally fractured reservoirs are composed of a rock matrix surrounded by a highly heterogeneous system of vugs and natural fractures. Over the past few decades, it has been observed that the characteristic behaviour of these reservoirs can be interpreted using an equivalent, homogeneous dual-porosity model as given in figure 3.4. [12]

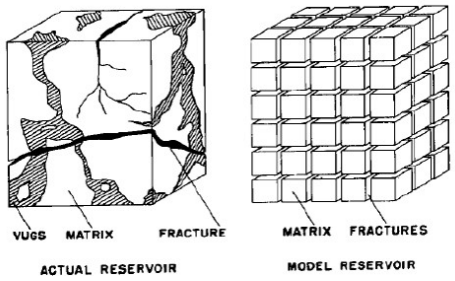

Figure 3.4: Simplification of a real naturally fractured reservoir in a idealized dual-porosity model. [12]

3.3.1. Constant pressure production

The objective of the production model is to analyze the decline curves of naturally fractured reservoirs at constant pressure production. The basic partial differential equations are based on a model originally presented by Warren & Root in 1963 and extended by several other authors (e.g. Cinco-Ley (1979)) to include wellbore storage and skin effect. The model is extended to analyze dimensionless flow rate for a well producing at a constant inner pressure from either a finite or an infinite dual-porosity system. The fundamental partial differential equations are [12]:

$$\frac{\partial^2 p_{fD}}{\partial r_D^2} + \frac{1}{r_D}\frac{\partial p_{fD}}{\partial r_D} = (1-\omega)\frac{\partial p_{mD}}{\partial t_D} + \omega\frac{\partial p_{fD}}{\partial t} \tag{3.1}$$

$$(1-\omega)\frac{\partial p_{mD}}{\partial t_D} = \lambda(p_{fD} - p_{mD}) \tag{3.2}$$

ω and λ are parameters defining reservoir and fluid properties. ω relates the storage capacity of fractures to the total storage of the system and is given by:

$$\omega = \frac{(\phi c)_f}{(\phi c)_f + (\phi c)_m} \tag{3.3}$$

$(\phi c)_f = Fracture\, storativity\, [-]$
$(\phi c)_m = Matrix\, storativity\, [-]$

λ controls the inter-porosity flow and is given by:

$$\lambda = \alpha \frac{k_m}{k_f} r_w^2 \tag{3.4}$$

where;

$$\alpha = \frac{4j(j+2)}{L^2} \tag{3.5}$$

$\alpha = Inter - porosity\, flow\, coefficient\, [\frac{1}{m^2}]$
$L = Characteristic\, dimension\, of\, a\, matrix\, block\, [m]$
$j = Number\, of\, normal\, sets\, of\, planes\, limiting\, the\, less - permeable\, medium\, (j = 1, 2, 3)[-]$
$k_f = Fracture\, permeability\, [D]$
$k_m = Matrix\, permeability\, [D]$
$r_w = Wellbore\, radius\, [m]$

For the closed outer boundary, the condition is:

$$\left.\frac{\partial p_{fD}}{r_D}\right|_{r_D = r_{eD}} = 0 \tag{3.6}$$

The dimensionless flow rate into the wellbore is given by:

$$q_D(t_D) = -\left(\frac{\partial p_D}{\partial r_D}\right)_{r_D = 1} \tag{3.7}$$

The dimensionless cumulative gas production is given by:

$$Q_D = \int_0^{t_D} q_D dt_D \tag{3.8}$$

A common method for solving equations 3.1 to 3.8 is the use of the Laplace transformation. This method transforms the equations into a system of ordinary differential equations which can be solved analytically. The resulting solution in the transformed space is a function of the Laplace variable, s, and the spatial variable, r_D. To invert the solution to real time and space, the inverse Laplace transformation is used. In order to find the inverse solution, an algorithm is used to approximate a numerical inversion of the Laplace transform solution. [12] The algorithm used to solve the problem has been presented by Stehfest (1970) and is modeled in MATLAB. Inverting for q_D and Q_D yields:

$$q_D(t_D) = \left(\frac{r_{eD}^2 - 1}{2}\right) \lambda e^{-\frac{\lambda}{1-\omega} t_D} \tag{3.9}$$

$$Q_D(t_D) = \frac{r_{eD}^2 - 1}{2} \left[(\omega - 1) e^{-\frac{\lambda}{1-\omega} t_D} + 1\right] \tag{3.10}$$

3.3.2. Dimensionless parameters

Dimenionless flow rate q_D Dimensionless flow rate q_D in the Warren & Root model is a function of dimensionless radius r_{eD} and storativity ratio ω ($q_D = f(r_{eD}, \omega)$) as illustrated in figure 3.5 and is given by the following formula:

$$q_D = \frac{115.74 q B \mu}{k_f h (p_i - p_w)} \tag{3.11}$$

$q = Flow\,rate\,[m^3/day]$
$h = Perforated\,interval\,[m]$
$B = Gas\,formation\,volume\,factor\,[-]$
$\mu = Gas\,viscosity\,[Pa \cdot s]$
$p_i = Reservoir\,pressure\,[bar]$
$p_w = Wellbore\,pressure\,[bar]$

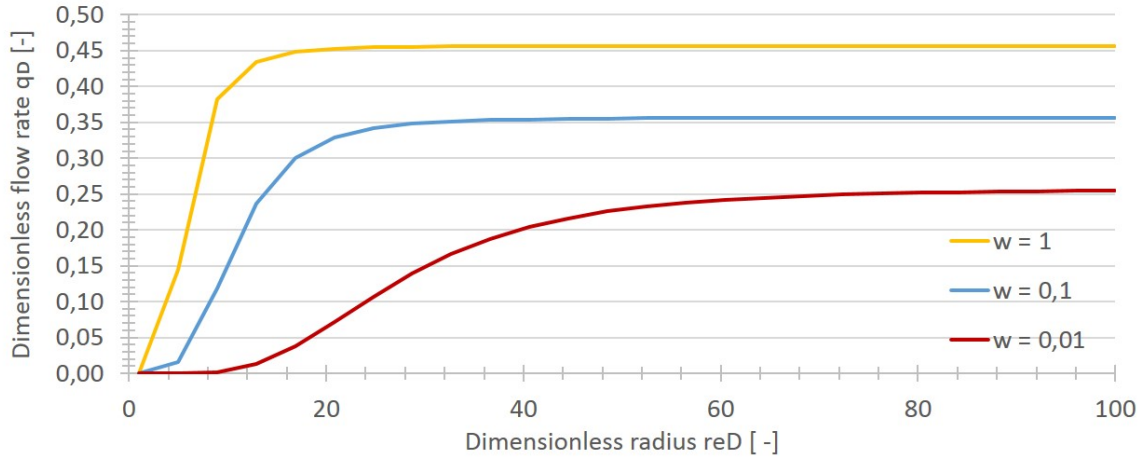

Figure 3.5: Dimensionles flow rate q_D function of dimensionless radius r_{eD} and storativity ratio ω. [13]

Dimensionless reservoir radius r_{eD} The dimensionless radius is given by the following equation:

$$r_{eD} = \frac{r_e}{r_w exp(-S)} \tag{3.12}$$

where;

$$r_e = \sqrt{\frac{GIIP \cdot B}{\pi h (\phi_m + \phi_f)}} \tag{3.13}$$

$r_e = Reservoir\,radius\,[m]$
$r_w = Wellbore\,radius\,[m]$
$S = Skin\,effect\,[-]$
$r_w exp(-S) = Effective\,wellbore\,radius\,[m]$
$GIIP = Gas\,Initially\,In\,Place\,[m^3]$
$h = Perforated\,interval\,[m]$
$\phi_m = Matrix\,porosity\,[-]$
$\phi_f = Fracture\,porosity\,[-]$

The dimensionless reservoir radius is a function of true reservoir radius and skin effect around the borehole. True reservoir radius is calculated using cumulative gas production and extrapolating it to gas initially in place ($GIIP$). The skin effect is an additional (positive or negative) pressure drop occurring at or close-by the well-face, and is responsible for the decrease or increase of the well productivity. In the case of negative skin, the effective wellbore radius accounts for the increase of sand face area exposed to reservoir flow due to acidizing, hydraulic fracturing or naturally fractured reservoirs. It

cannot be measured directly, but it can be calculated using equation 3.12 and 3.13. Therefore, skin factor should be considered qualitatively rather than quantitatively. First, skin effect is assumed to be -4.8, equal to the average skin effect from well-test reports of the given wells (figure 3.6). Skin effect is chosen such that the relation between dimensionless radius r_{eD} and gas initially in place ($GIIP$) becomes power-law (figure 3.6). Skin effect ranges between -5.2 and -3.6. Skin effects are also listed in appendix A.2.

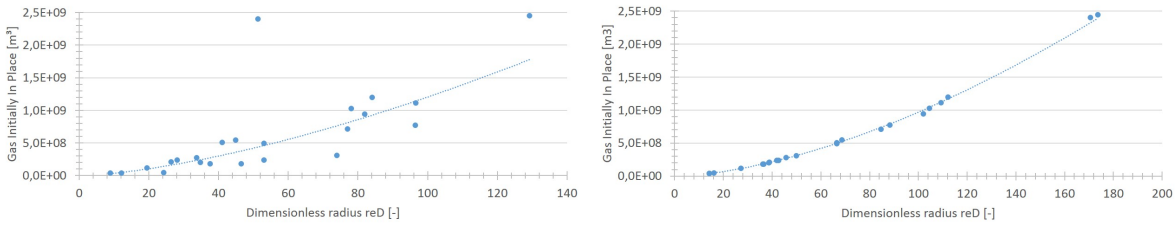

Figure 3.6: $GIIP - r_{eD}$ relation for constant skin effect $S = -4.80$ (left). Power-law relationship between dimensionless radius r_D and gas initially in place $GIIP$; $GIIP = 540122 r_{eD}^{1.6393}$ (right). Blue dots represent the calculated value for each specific well used in the Warren & Model.

Combining the obtained equation for GIIP and 3.13 gives the formula for reservoir radius r_e:

$$r_e = \sqrt[0.367]{\frac{540122 \cdot B}{\pi(\phi_m + \phi_f)hr_w^2}} \tag{3.14}$$

Combining equation 3.14 and 3.12 gives the formula for dimensionless radius r_{eD}:

$$r_{eD} = \frac{\sqrt[0.367]{\frac{540122 \cdot B}{\pi(\phi_m+\phi_f)hr_w^2}}}{r_w exp(-S)} \tag{3.15}$$

3.3.3. Examples of varying parameters

Examples for varying input parameters for the Warren & Root Model are illustrated in figure 3.7. The examples are obtained by implementing the Warren & Root model description by Da Prat et al. in MATLAB. The production profile depends on the storativity ratio and the inter-porosity flow explained in the following paragraphs:

Storativity ratio When a reservoir solely constitutes of fractures (i.e. $\omega = 1$), the high initial dimensionless flow rate is sustained until the whole reservoir is depleted and dimensionless flow rate decreases to zero (figure 3.7). Decreasing the fracture storativity (i.e. decreasing storativity ratio) will result in an earlier decrease in dimensionless flow rate and transition to a lower flow rate sustained by matrix production.

Inter-porosity flow The inter-porosity flow will increase when matrix permeability increases or when fracture permeability decreases. When the ability of fluid to flow from matrix system to the fracture system is high (i.e. inter-porosity flow is high), the total system production equals the initial dimensionless flow rate and the initial flow rate can be sustained until the end of production. If the inter-porosity flow is very low, the fluid struggles to flow from the matrix system into the fracture system and the high initial flow rate can not be sustained and flow rate drops to a lower flow rate which can be sustained by the matrix system (figure 3.7).

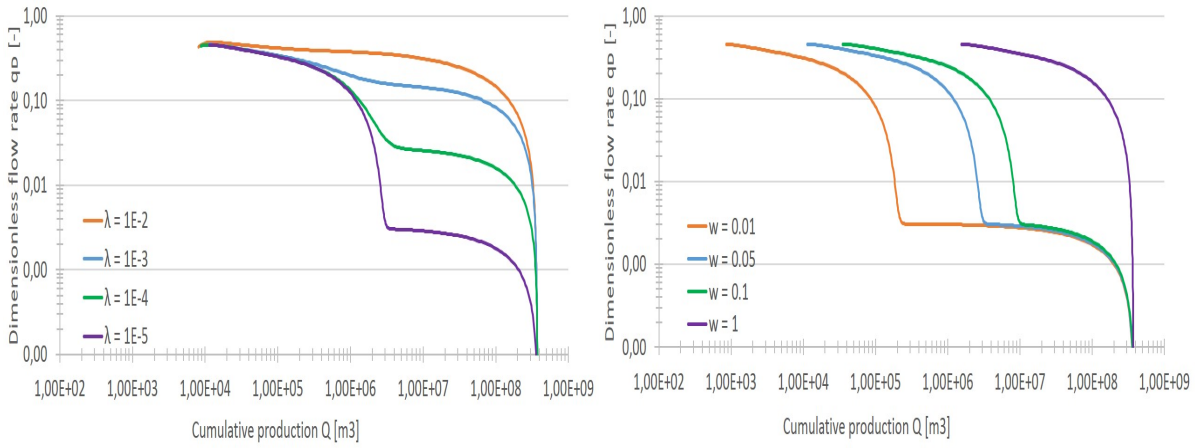

Figure 3.7: Left: Varying interporosity flow λ, $r_{eD} = 25$. Right: Varying storativity ratio ω, $r_{eD} = 25$. Solution is obtained by the implementation of the description for the Warren & Root model by Da Prat et al. in MATLAB.

3.4. Depositional model

The depositional model is to obtain:

- **Matrix porosity ϕ_m and matrix permeability ϕ_m**

The Zechstein-2 Carbonate Member follows the relief created by the Zechstein-1 Formation (Figure 2.6). The Zechstein-1 Formation is mostly deposited along the Southern Permian basin margins due to variation in gypsum accumulation between basin and shallow waters (see chapter 2). Therefore, the thickest Zechstein-1 accumulations can be found along the margins of the basin. The Zechstein-1 Formation relief was the basis for the accumulation of the Zechstein-2 Carbonate Member where platform and shelf facies were deposited in the shallow waters on top of the thick Zechstein-1 Formation and basinal facies towards the center of the basin. Therefore, the thickest accumulations of the Zechstein-2 Carbonate Member can be found on top of the thickest Zechstein-1 Formation accumulations. The combined part of the Lower Zechstein Group (Zechstein-1 Formation + Zechstein-2 Carbonate Member) is informally known as the 'Basal Zechstein Unit'. The thickness of this unit relates to the different depositional environments as explained above; the thickest unit can be found where Zechstein-1 and Zechstein-2 members were deposited in shallow waters (i.e. Zechstein-1 anhydrite deposits and thick Zechstein-2 carbonate platform facies, respectively). The thickness of the 'Basal Zechstein Unit' is the smallest were little or no deposition occurred (basinal facies towards no deposition in the center of the basin). This means that the thickness of the 'Basal Zechstein Unit' relates to a certain depositional environment and thus a specific facies. Van der Sande et al. combined these findings with core descriptions and porosity measurements and assigned specific facies to this thickness relation. The result of this study shows a distinct relation between the thickness of the Zechstein-2 Carbonate Member and that of the 'Basal Zechstein Unit' and the corresponding facies (figure 2.6 and A.2). [8] Generally, the porosity shows an increase from basin towards platform and therefore shows a similar relation to the thickness of the 'Basal Zechstein Unit' (figure 3.8 and figure A.3). Simple matrix porosity-permeability relationships are constructed from core measurement from 11 different wells in the area of interest (figure 3.9) in combination with the study by Van der Sande et al.. A list of all the wells with core measurements used in this analysis can be found in appendix A.1.

3.4.1. Matrix porosity

The matrix porosity trend corresponds to the study done by Van der Sande et al.. The porosity within the area of interest increases towards the platform edge (figure 3.8). The yellow points in the figure represent the median measured core porosity with standard deviation error bars. The dotted red line corresponds to the maximum matrix porosity by Van der Sande et al. and core measurements from the area of interest used in this study. The brown points represent the best-fit input matrix porosity used in the Warren & Root model for a specific well.

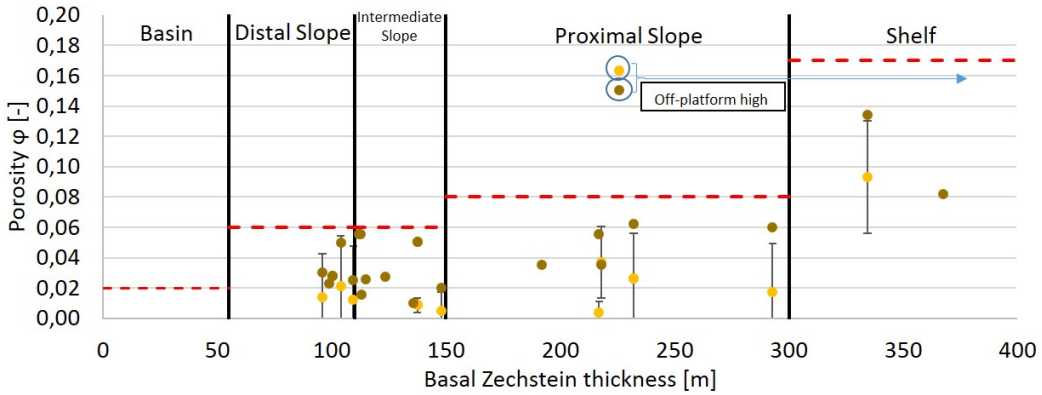

Figure 3.8: Porosity relation to Basal Zechstein thickness from core plug measurements (www.nlog.nl) in area of interest, trend corresponds to study by Van der Sande et al. Error bars show standard deviation in measured porosity from different core plugs of a single well. The dotted red line indicates the maximum possible porosity for a specific facies corresponding to the study by Van der Sande et al.. The outlier is explained by an erosional surface of the 'Basal Zechstein Unit' which decreased the total thickness and the less extensive deposition of the total unit because of its geographical position as an off-platform high located into the basin.

3.4.2. Matrix permeability

Matrix permeability measurements are executed by the NAM on several cores and the results are shown in figure 3.9. Wells are plotted as points with corresponding standard deviation represented by error bars. The trend-line corresponds to the manual best-fit power-law porosity-permeability relation used as input for the Warren & Root model. At low porosity values, the measurements show very high permeability values (greater than 10 mD), which is highly doubtful since higher porosity values (around 15%) do not even reach these high permeability values. These values are assumed to be erroneous either due to exceeding the minimum limit of the used equipment or by specifically chosen permeability measurement on 'special' core plugs (e.g. vuggy porosity, fracture porosity, etc.) of which the connected pore volume is much larger than primary connected pore volume. These 'special' core plug measurement do not belong to the matrix permeability and are therefore not considered for matrix permeability.

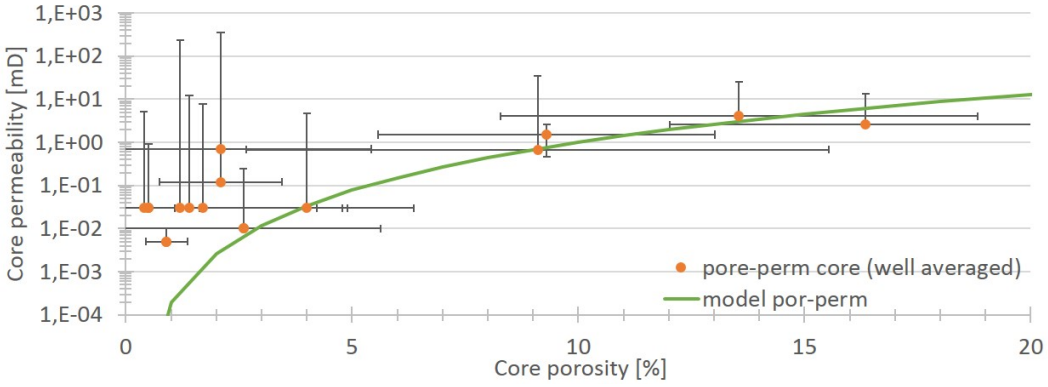

Figure 3.9: Porosity-permeability relation core plug measurements (www.nlog.nl) wells in area of interest. Error bars show standard deviation in measured permeability from different core plugs of a single well. The green line (model) is used as an average porosity-permeability correlation for the Warren & Model. Matrix permeability $k_m = 2 \cdot 10^{-4} \phi_m^{3.7}$

3.5. Fracture network model

The fracture network model is to obtain:

- **Fracture porosity ϕ_f and fracture permeability k_f**

Fracture networks are a main controlling parameter on reservoir performance. Understanding and predicting these patterns is viable for the development of a field. The importance of fractures is demon-

strated by previous drilled wells within the area which encountered major open fractures (indicated by significant mud-losses during drilling) resulting in productivities exceeding $0.5 \cdot 10^6\ m^3/d$ and up to $6.5 \cdot 10^6\ m^3/d$ [9]. Previous core analysis studies show that N-S oriented and NNE-SSW (sub-)vertical oriented fractures are open and show the highest contribution to reservoir quality [9].

3.5.1. Assumptions

Due to real-life complications as explained above, some assumptions have to be taken into account to predict the fracture network;

- Fractures are systematic, planar and non-convex
- Fractures abide the parallel-plate model

3.5.2. Lateral fracture density and aperture distribution

Fracture density distribution Fractures provide storage capacity and high permeability pathways for fluid flow in naturally fractured rocks where characteristics are controlled by the properties of the fracture. Spatial variations in fracture density are a consequence of the way in which strain is accumulated across a region. The resulting fracture network is a complicated interaction between regional stress fields and local modification around developing structures. Many geological factors that might influence the fracture density include fault damage zones, shear reactivation of existing fractures, fold hinges, mechanical layer thickness and mechanical layer hardness. Spatial variation in fracture density is therefore a result of two important components; variation of facies or localized concentration of deformation (e.g. faults). Generally, fault zone structures can be characterized by a high-strain main gouge zone along which most fault displacement occurs and is often in the order of tens of meters wide. The fault core zone is surrounded by a damage zone which can reach widths up to several hundred of meters. This damage zone is subsequently surrounded by undeformed host rock. The ratio between the spacing of the boundary faults of the Lauwerszee Trough and the spacing of associated antithetic Riedels ranges from approximately 10:1 to 20:1. Other studies on analogue fractured outcrops show the same spacing ratio between wrench faults and the associated fracture systems. The distance between the E-W trending boundary faults of the Emmen field is on average circa 5 km. Applying above ratios result in fracture spacings of approximately 250-500 m for the NNW-SSE striking fracture set. The spacing of individual micro-fractures is in the order of decimeters to meters. [9]

Fracture aperture distribution The intention of an aperture model is to give an estimate of the probability distribution of aperture sizes [14]. Fracture aperture data (e.g. core measurements, borehole images) is very scarce in the Zechstein-2 Carbonate Member. For the NNW-SSE striking fracture set with spacing ranging from 250 to 500 m, apertures of 25-35 cm have been recorded using CBIL log analysis in Zechstein reservoirs. [9] It is often useful to use other studies as potential analogue data sets. Ortega et al. presented a study about linking aperture and spacing relations from carbonates in Mexico, which shows a very clear power-law distribution previously used in Zechstein studies by Geospatial Research Limited [15]. These analogue studies have been used as an input for the fracture modeling and corrected to match with the core fracture analysis and study by Frikken et al. [9] (Figure 3.10). Fracture density is related to fracture aperture by the following equation[14] and corrected to match the conducted core fracture analysis and fracture study by Frikken et al. [9] (Figure 3.10):

$$D_f = 0.4 \cdot b^{-0.8} \tag{3.16}$$

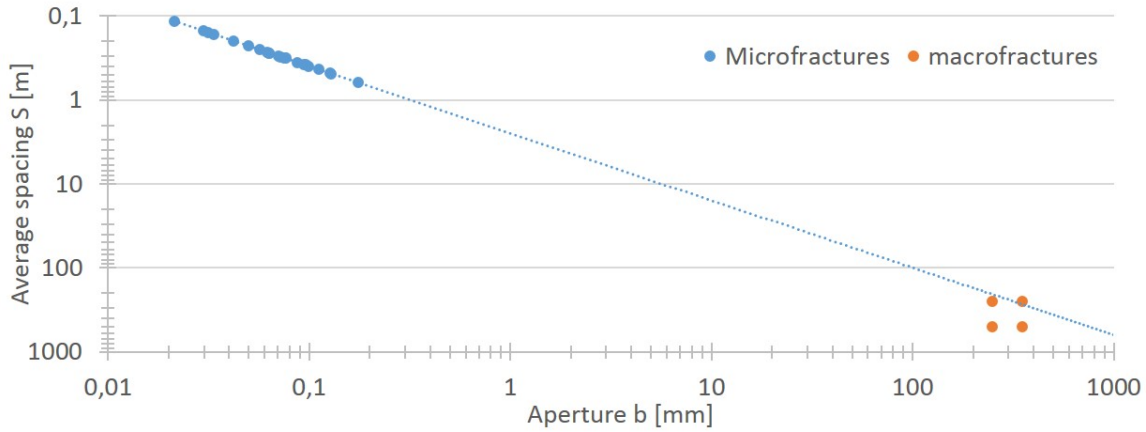

Figure 3.10: Fracture spacing-density correlation. Blue dots represent the calculated value for each specific well used in the Warren & Model. Orange dots represent spacing-density range for macrofractures.

3.6. Fracture modeling

Fracture permeability k_f The equation for velocity of volumetric flow, combined with Darcy's law, provides a simple approach to estimate fracture density and aperture from permeability. For a successful transformation from flow rate to dimensionless flow rate, the pressure drop and fracture permeability in the system have to be known. Fracture permeability is a parameter of the reservoir and necessary for analysis. Pressure drop is a function of the wellbore system and surface facilities and not dependent reservoir properties. Both parameters are unknown so the analysis is done with boundary conditions limiting the pressure drop between reservoir and wellbore with $\Delta P = 100$ bar. Thus, it is assumed that the influence of the differences in pressure drop between the wells is much smaller than the reservoir properties affecting fluid flow. It is evident from equation 3.11 that the initial flow rate is controlled by the fracture permeability. The Warren & Root model abides this relation through equation 3.17 as illustrated in figure 3.11.

$$k_f = \frac{115.74 q B \mu}{q_D h \Delta P} \tag{3.17}$$

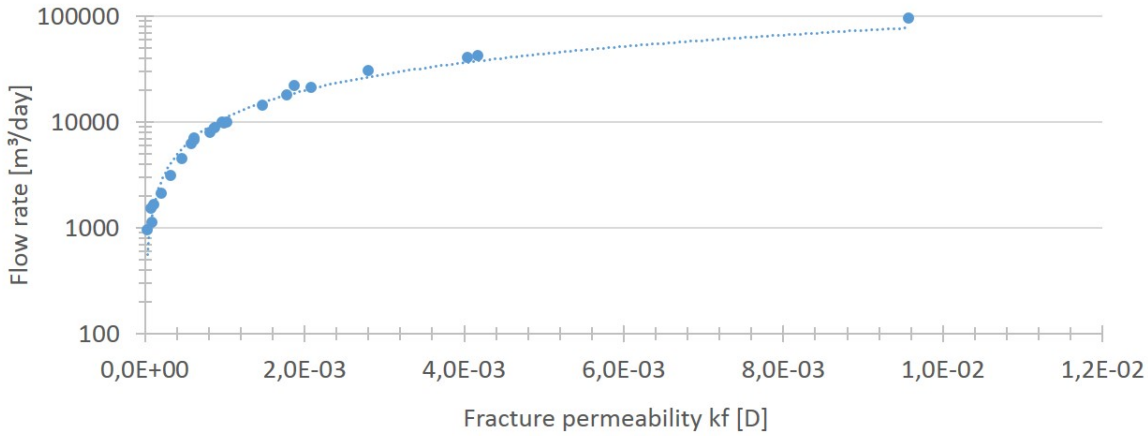

Figure 3.11: Flowrate per meter reservoir per day versus fracture permeability. Blue dots represent the calculated value for each specific well used in the Warren & Model.

3.6.1. Fracture aperture

The 'Cubic Law' provides a simple relation between the hydraulic conductivity and the fracture aperture and density (Figure 3.12) for a given fluid in a parallel-plate model. The fracture permeability with an

aperture b is given by:

$$k_f = \frac{b^2 \phi_f}{12} = \frac{b^3 D_f}{12} \tag{3.18}$$

$k_f = Fracture\,permeability\,[m^2]$
$b = Fracture\,aperture\,[mm]$
$\phi_f = Fracture\,porosity\,[-]$
$D_f = Fracture\,density\,[\#/m]$

rewriting for aperture b and implementing equation 3.16:

$$b = \sqrt[2.2]{\frac{12 k_f}{0.4 \cdot 1000^{-0.8}}} \tag{3.19}$$

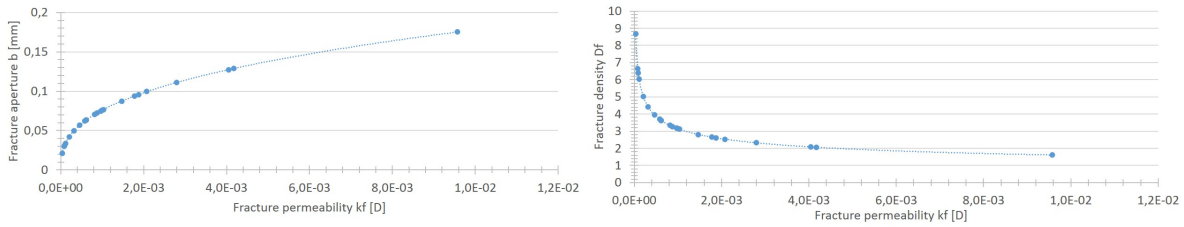

Figure 3.12: Left: Aperture-permeability relation. Right: Density-permeability relation. Blue dots represent the calculated value for each specific well used in the Warren & Model.

Fracture porosity can be calculated using the following equation (figure 3.13):

$$\phi_f = b \cdot D_f \tag{3.20}$$

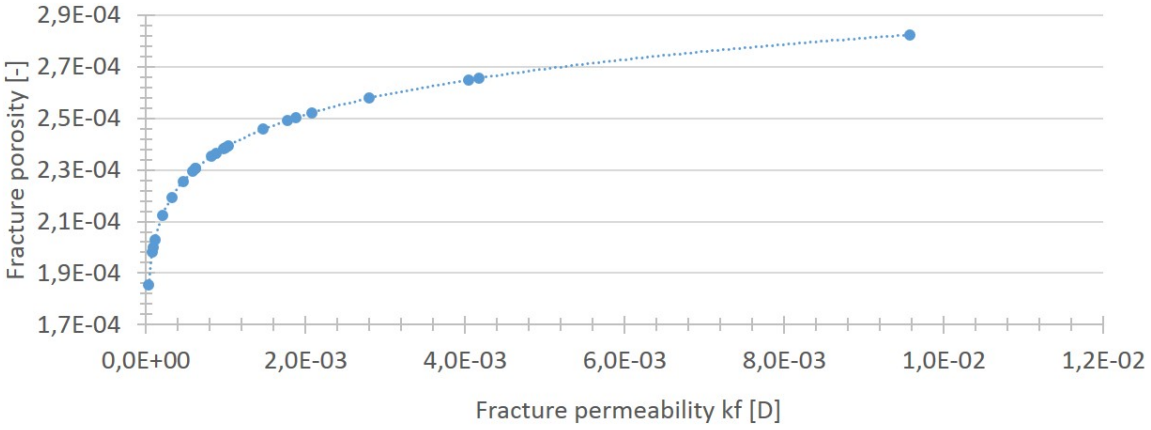

Figure 3.13: Fracture porosity-permeability relation. Blue dots represent the calculated value for each specific well used in the Warren & Model.

3.6.2. Input parameters iteration

To determine the fracture permeability in the Warren & Root model, the dimensionless flow rate has to be calculated. The initial dimensionless flow rate is a function of dimensionless radius and storativity ratio ω and therefore a function of fracture aperture (i.e. fracture porosity):

$$q_D = f(r_{eD}, \omega) \rightarrow \omega = f(\phi_f, \phi_m) \rightarrow \phi_f = f(b, D_f) \rightarrow b = f(k_f) \tag{3.21}$$

Thus, calculating dimensionless flow rate q_D requires storativity ratio ω which requires fracture aperture, while for fracture aperture fracture permeability is required:

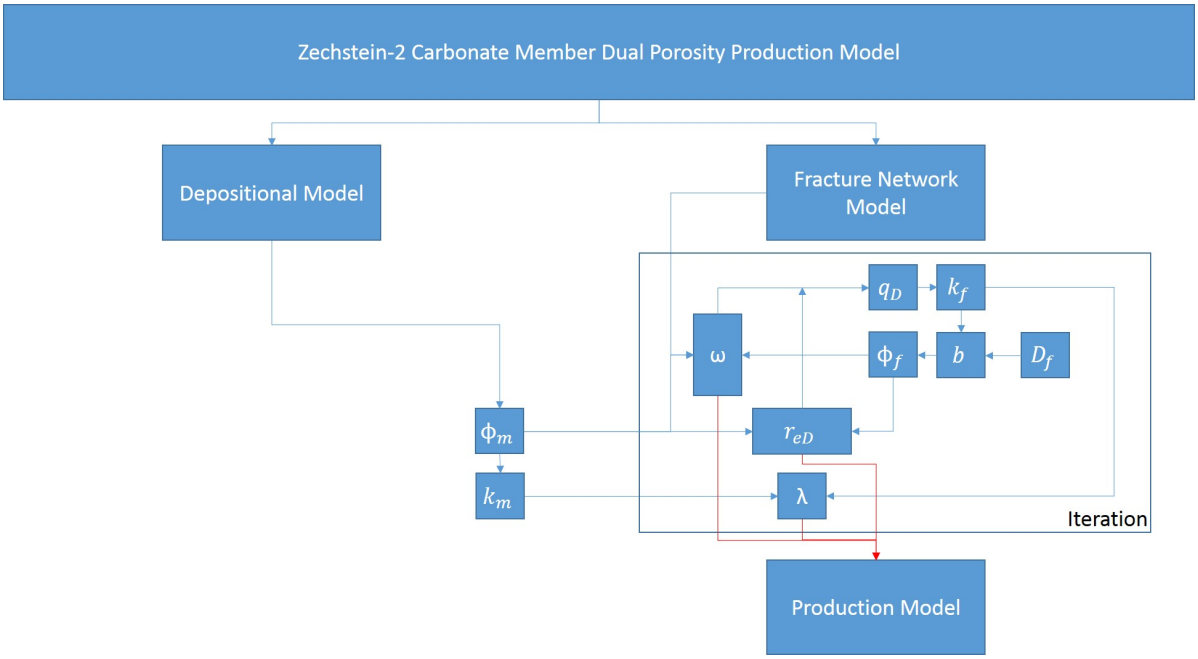

Figure 3.14: Iterative proces to combine Warren & Model, cubic law and fracture density-aperture relation. A storativity ratio ω is assumed to start the iteration.

4

Results

Zechstein-2 Carbonate Member is highly variable in production behavior. Correctly allocating specific reservoir characteristics gives some insight in the production behavior and possibility in predicting initial flow rate, reservoir size and decline curve. The main parameters controlling production behavior are the involved facies and fracture networks. Predicting both before drilling (i.e. with the use of seismic map interpretation) is essential for the successful exploration of hydrocarbons. The main parameters are derived from the best match decline curve for each specific well. Best decline curve matches are given in appendix B.1.

4.1. Reservoir radius

The connected gas volume which can possibly be produced from a certain reservoir depends on the reach of the well (i.e. dimensionless reservoir radius r_{eD}). Connected gas volume is dependent on reservoir characteristics and structural features of the reservoir. In this model, structural features (i.e. reservoir boundaries) are not taken into account. Reservoir radius is dependent on two main reservoir characteristics contributing to reservoir size:

- Matrix porosity ϕ_m
- Fracture porosity ϕ_f

Matrix porosity Matrix porosity is a function of diagenesis and depositional texture. Diagenesis mostly affects proximal slope and shelf facies through leaching and dissolution. Depositional texture is most favorable for proximal slope to shelf facies due to the presence of larger particles with respect to distal- to intermediate slope facies (oolitic, pelletoidal, pisolitic, etc.). Porosity increases from basin towards the margin of the platform (Figure 3.8) resulting in highest connected volumes at the platform margin (Figure 4.11).

Fracture porosity Fracture porosity is the product of the fracture density and fracture aperture. Aperture is the main controlling parameter on fracture porosity. Thus, increasing fracture aperture has the highest impact on fracture network connectivity resulting in the largest connected gas volume. The present-day maximum principal stress is largely parallel to the extensional open fracture trend or the antithetic Riedel shear fractures and has probably contributed to their preservation. The fracture sets strike approximately NW-SE to N-S, respectively, and are the most important fracture sets for reservoir permeability (Figure 2.11). [9]

Flow rate The total initial flow rate is dependent on the fracture porosity, matrix porosity and the net gas column present in the well. Increasing fracture porosity (i.e. increasing fracture aperture) increases fracture permeability and therefore significantly increases flow rates (Figure 3.11). High inter-porosity flow values for high matrix porosity reservoirs (e.g. shelf facies) enables the matrix system to support the fracture system on high flow rates throughout the production lifetime of a well (Figure

3.7). Evidently, large net gas column will lead to a higher total flow rate. Generally, this means that the wells having the highest initial flow rate will have the highest cumulative gas production. Power-law trends show best fits for each specific facies. Figure 4.2 shows that this relation is valid for all facies with coefficients of determination of $R^2_{Shelf} = 0.9539$, $R^2_{Proximal} = 0.7941$, $R^2_{Intermediate} = 0.8645$ and $R^2_{Distal} = 0.6269$.

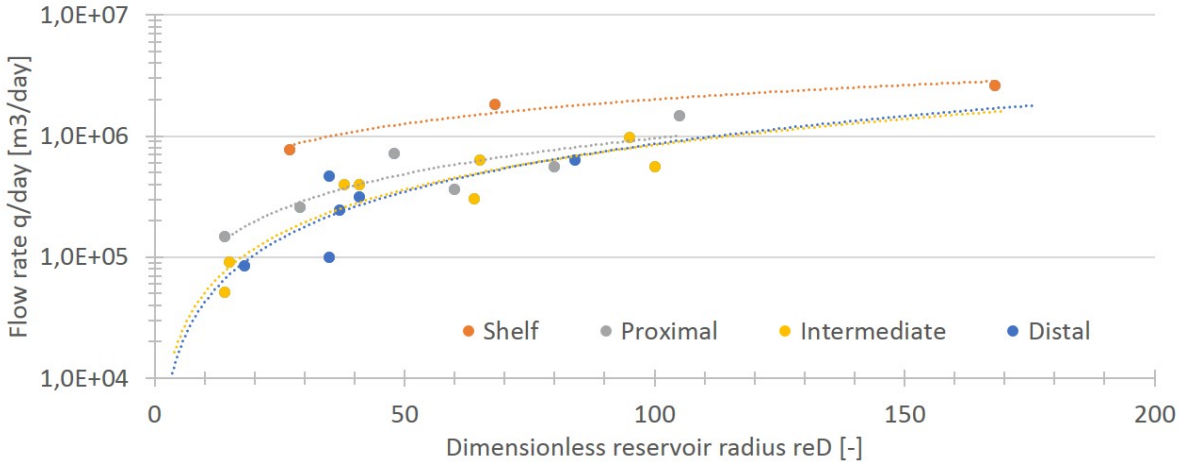

Figure 4.1: Total flow rate (function of fracture porosity, matrix porosity and net gas column) relation to dimensionless reservoir radius. Trend lines show best-fit power-law curves for each specific facies.

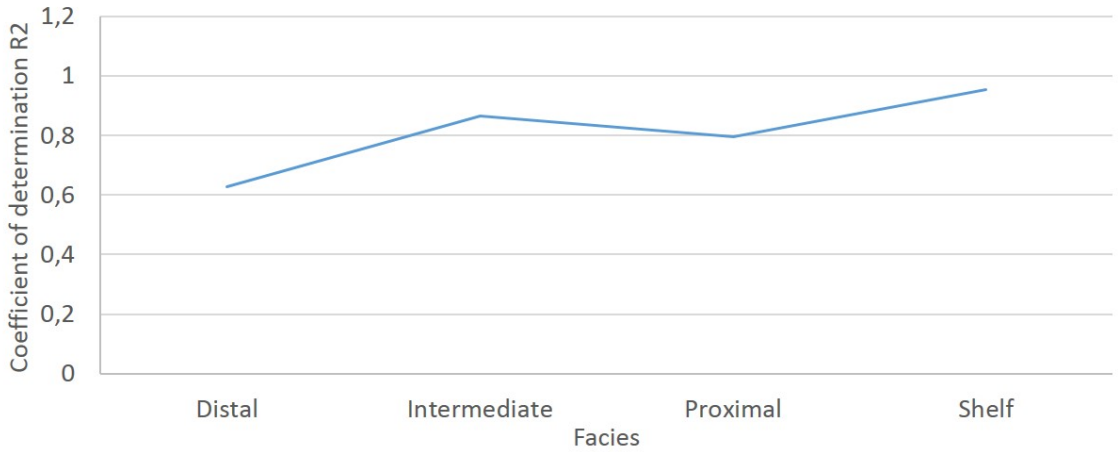

Figure 4.2: Coefficient of determination for flow rate versus reservoir radius of each specific facies with shelf facies $R^2 = 0.9539$, proximal slope facies $R^2 = 0.7941$, intermediate facies $R^2 = 0.8645$ and distal slope facies $R^2 = 0.6269$.

4.1.1. Fracture porosity

Fracture aperture is the main controlling parameter for permeability (Figure 3.12). Increasing fracture aperture means higher fracture porosity thus higher permeability and therefore larger connected gas volumes (Figure 4.3). Reservoir size of distal- to proximal slope facies shows a good relation to fracture porosity while shelf facies does not relate to fracture porosity (Figure 4.4) with coefficients of determination of $R^2_{Shelf} = 0.0526$, $R^2_{Proximal} = 0.5640$, $R^2_{Intermediate} = 0.6897$ and $R^2_{Distal} = 0.6068$. This means that fracture porosity is a main controlling factor for reservoir size only for distal- to proximal slope facies. Fracture porosity for shelf facies is not a main controlling parameter on reservoir size.

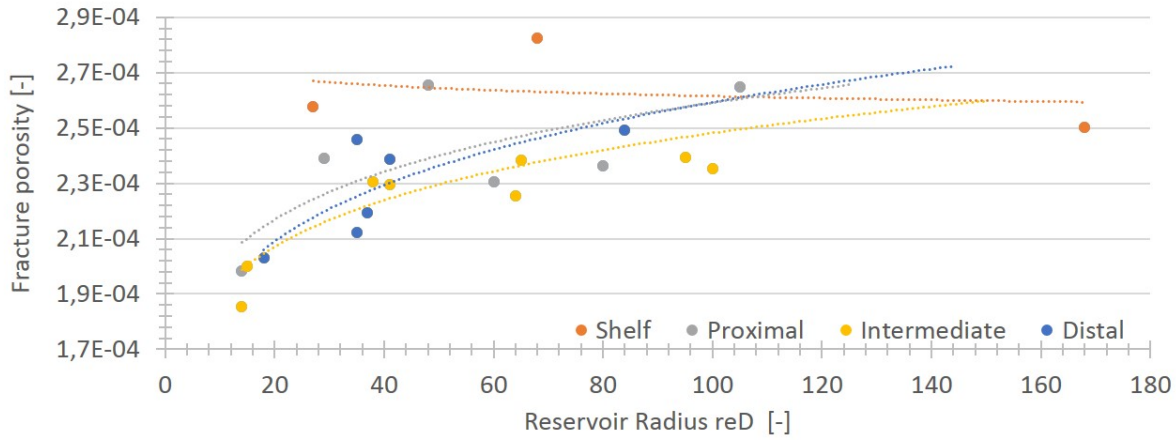

Figure 4.3: Fracture porosity relation to dimensionless reservoir radius. Trend lines show best-fit power-law curves for each specific facies.

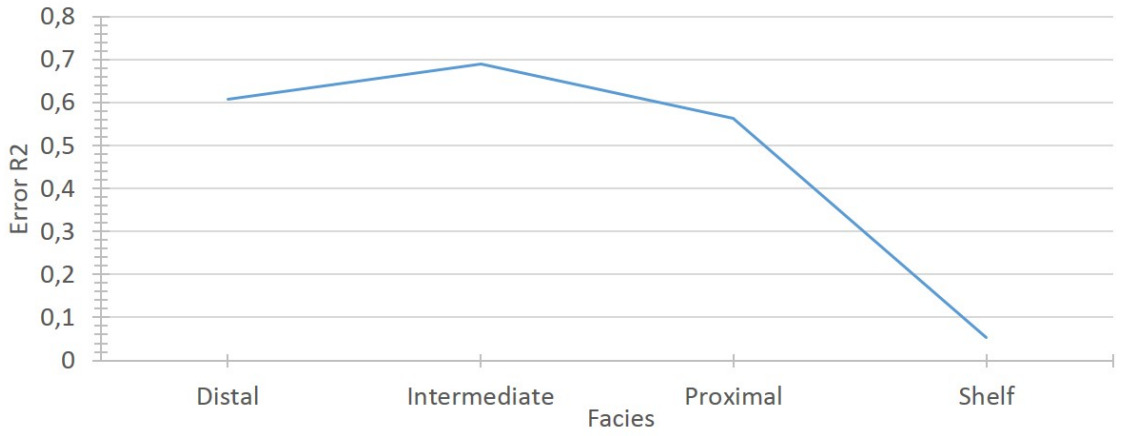

Figure 4.4: Coefficient of determination for fracture porosity versus reservoir radius for each specific facies with shelf facies $R^2 = 0.0526$, proximal slope facies $R^2 = 0.5640$, intermediate facies $R^2 = 0.6897$ and distal slope facies $R^2 = 0.6068$. Fracture porosity is a main controlling parameter for distal- to proximal slope facies. Shelf facies reservoir size is not controlled by fracture porosity.

4.1.2. Fracture density

The fracture networks present in the Zechstein-2 Carbonate Member are modeled using the 'cubic law' equation and the spacing-density relation given in figure 3.10. Spatial variation in fracture density is a result of variation in facies or localized concentration of deformation (e.g. faults). Fracture density has an inverse relation to reservoir size; high fracture densities result in small connected gas volumes, while low fracture densities tend to increase the connected gas volume (Figure 4.5). For distal- to proximal slope facies the correlation is clear. Fracture density for shelf facies does not have an influence on the connected gas volume.

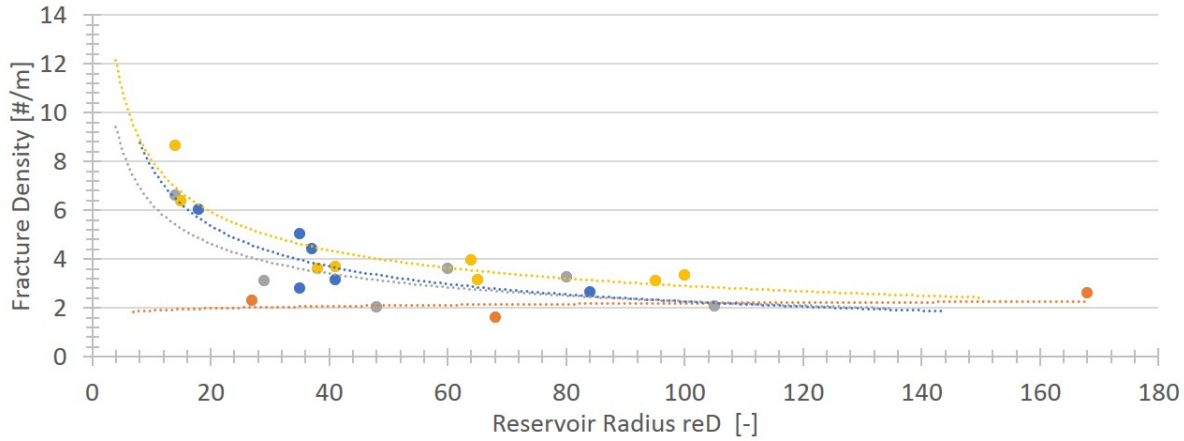

Figure 4.5: Fracture density relation to dimensionless reservoir radius.

4.1.3. Fracture aperture

Generally, fracture aperture increases with decreasing fracture density. Therefore, fracture aperture shows an inverse relation compared to fracture density. Large fracture apertures tend to have the largest connected gas volume while small fracture apertures result in small connected gas volume (Figure 4.6). For distal- to proximal slope facies the correlation is clear, shelf facies reservoir size does not show a relation to fracture aperture.

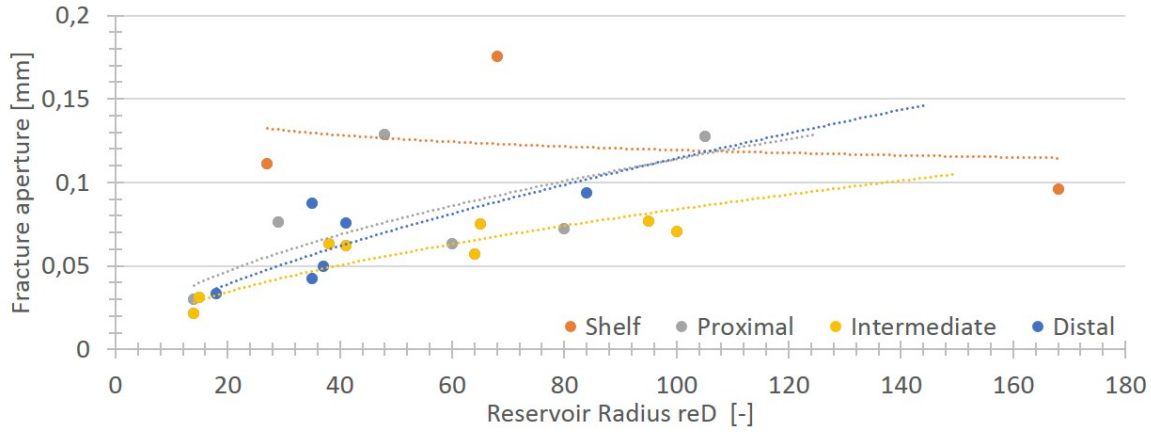

Figure 4.6: Fracture aperture relation to dimensionless reservoir radius.

4.2. Influence of large open fault systems

The influence of large open fault systems is determined by measuring the distance to the nearest NW-SE- to NS-trending faults. These faults coincide with the present-day horizontal maximum principle stress and are interpreted as extensional or antithetic Riedel shear faults (Figure 2.11). This present-day maximum principal stress is largely parallel to the extensional open fracture set and is therefore used as a possible indicator for open fracture networks. Exact configuration of the fault zone deformation depends on the properties of the host rock and fault zone (e.g. porosity, composition and the amount of fault slip). In low porosity host rock the fault zones are generally considered to be flow barriers due to the presence of finely grained material and clay content. Fault zones in high porosity host rock may have inverse characteristics with enhanced fluid flow parallel to the fault core zone. [15] Wells penetrating distal- to proximal slope facies close to these open faults show lower flow rates compared to wells drilled further away from the fault (Figure 4.7). This indicates that these large fault systems act as a flow barriers. Wells penetrating shelf facies have higher flow rates close to a fault system compared to wells drilled further away from a fault. This indicates that these large fault systems impede flow for high porosity facies.

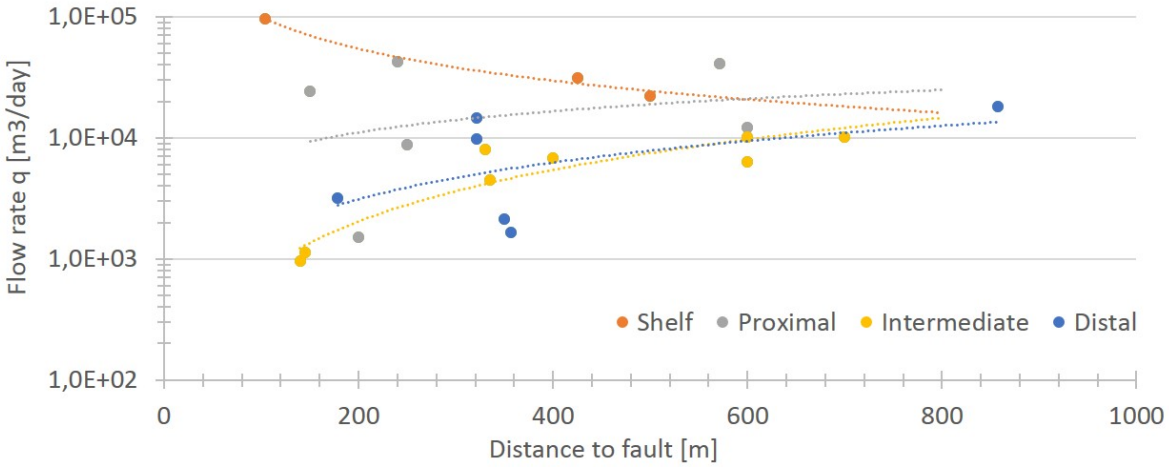

Figure 4.7: Flow rate as a function of distance to fault.

4.2.1. Fracture porosity

Fracture porosity decreases towards the nearest open fault for distal- to proximal slope facies. Shelf facies show an increase in fracture porosity (Figure 4.8). Distal slope facies tend to have the lowest fracture porosity for a given distance to fault, while shelf facies have the highest fracture porosity. Distal- to proximal slope shows a clear relation to the nearest fault while the distance to the nearest fault has an inverse relation to fracture porosity for shelf facies.

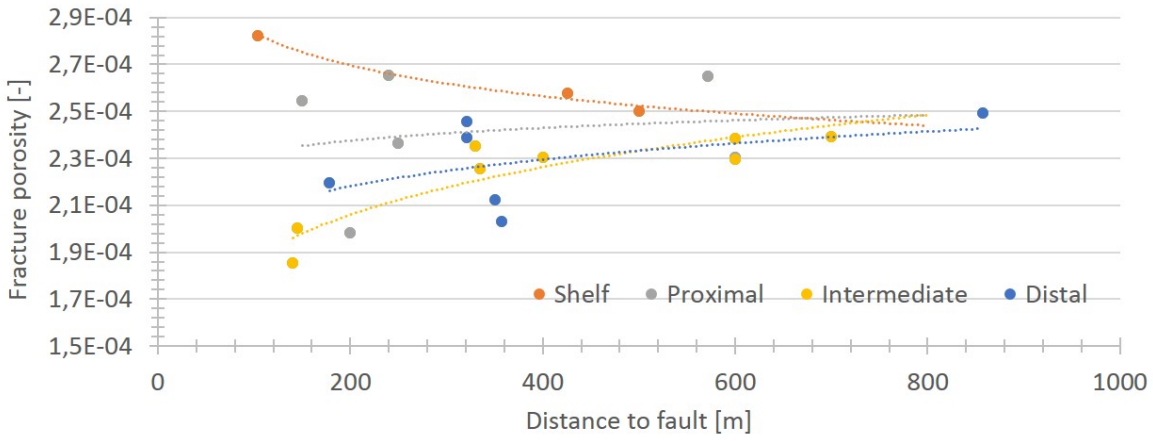

Figure 4.8: Fracture porosity as a function of distance to fault with decreasing fracture porosity towards the fault.

4.2.2. Fracture density

Spatial fracture density distribution is controlled by a variation in facies and faults. As can be seen in figure 4.9, fracture density decreases with increasing distance to the nearest fault. Distal- and intermediate slope facies have a higher fracture density for a given distance to the nearest fault compared to proximal slope and shelf facies which have the lowest fracture density. Distal- to proximal slope facies show a clear relation with the distance to the nearest open fault. Shelf facies does not show an increase in fracture density towards open fault zones, but even a small decrease.

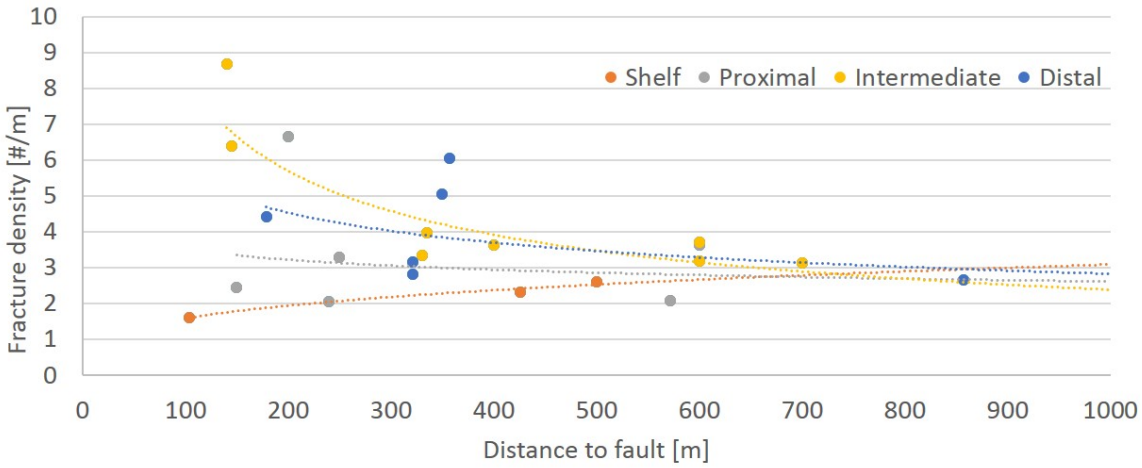

Figure 4.9: Fracture density as a function of distance to fault with increasing density towards the fault zone.

4.2.3. Fracture aperture

Fracture apertures show a reverse relation to distance to the nearest open fault compared to fracture density (Figure 4.10. Shelf facies tend to have the highest apertures at a given distance to the nearest fault compared to distal- to proximal slope facies, which have the smallest apertures. Apertures of shelf facies have an inverse relation compared to distal- to proximal slope facies with distance to the nearest open fault.

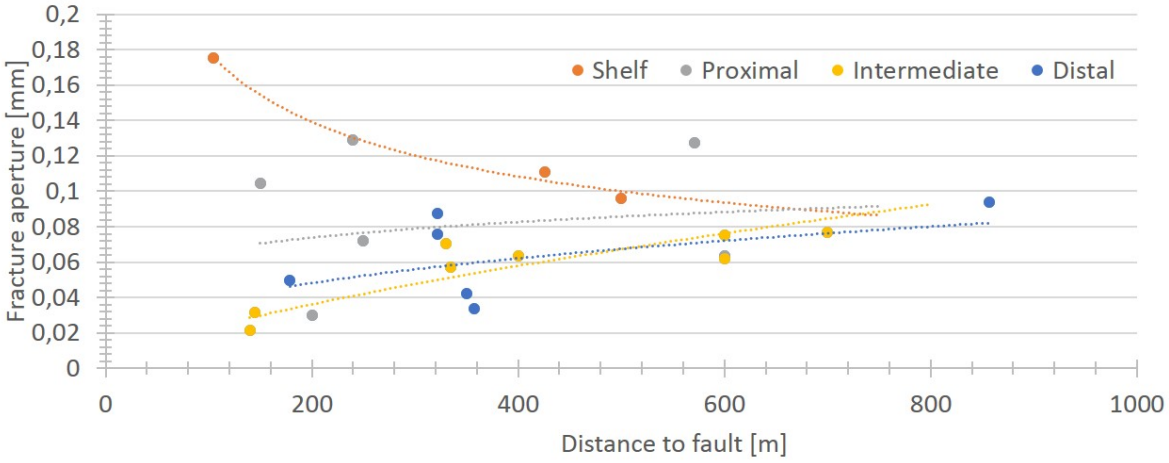

Figure 4.10: Fracture aperture as a function of dinstance to fault with decreasing aperture towards the fault zone.

4.3. Warren & Root model

The Warren & Root model gives a simplified production decline model for naturally fractured carbonate reservoirs. It is defined by three main parameters including storativity ratio, inter-porosity flow and dimensionless reservoir radius. These parameters are mostly dependent on the type of facies present and the fracture network model.

4.3.1. Reservoir size

Facies are a main controlling parameter for reservoir size as depicted in figure 4.11. Naturally, high porosity reservoirs (shelf facies) tend to have a higher connected volume than lower porosity reservoirs (distal slope facies). The variation in reservoir size exists due to heterogeneities within a specific facies and the varying extent of the fracture network.

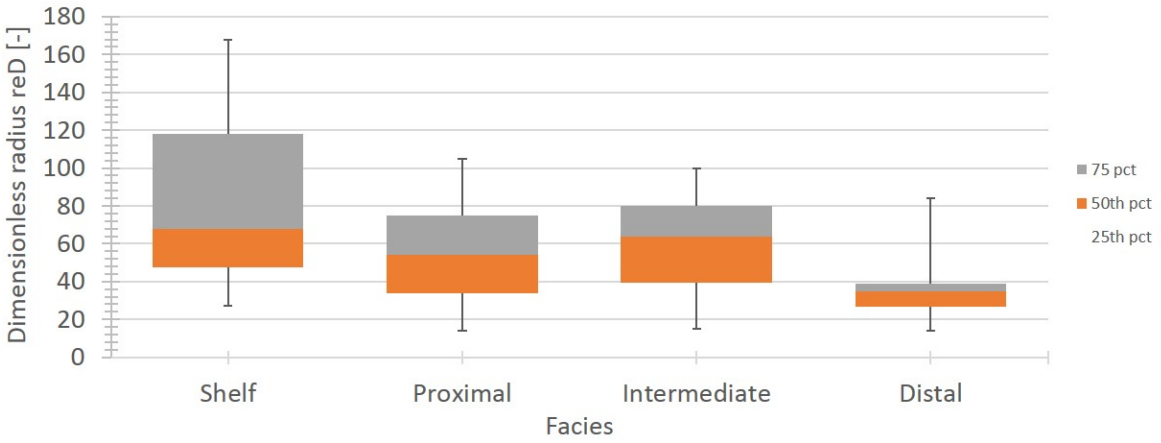

Figure 4.11: Dimensionless radius for specific facies. nr of wells: Shelf = 3. Proximal = 7. Intermediate = 9. Distal = 4.

4.3.2. Initial flow rate

The highest cumulative gas production is achieved for wells with the highest initial flow rates (Figure 4.1). Shelf facies generally have the highest initial flow rate due to high porosity (often > 15%) and good connected fracture networks. Low porosity facies (distal- to proximal slope facies) generally have lower initial flow rates with decreasing flow rates towards the basin.

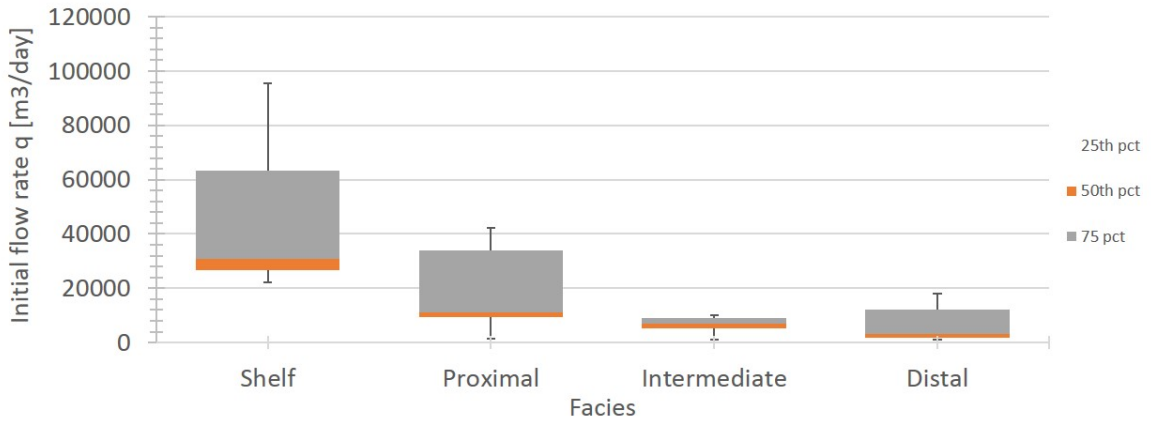

Figure 4.12: Initial flow rate for specific facies. nr of wells: Shelf = 3. Proximal = 7. Intermediate = 9. Distal = 4.

4.3.3. Storativity ratio

The storativity of the fracture networks is a function of the fracture porosity and the matrix porosity. As matrix porosity increases towards the platform fringe, the storativity ratio will consequently decrease (Figure 4.13). The boundary values for storativity ratio are therefore mainly defined by the maximum and minimum matrix porosity of a specific facies.

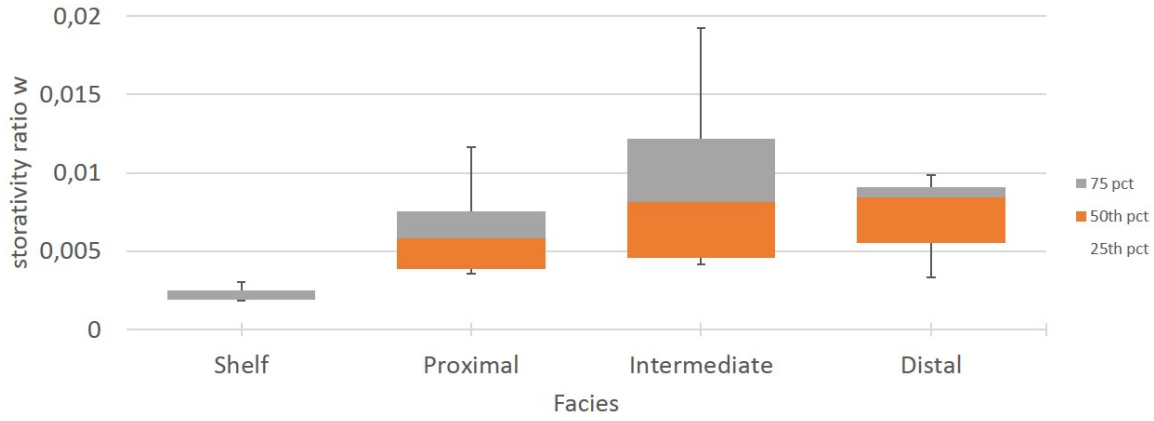

Figure 4.13: Storavity ratio range for specific facies. nr of wells: Shelf = 3. Proximal = 7. Intermediate = 9. Distal = 4.

4.3.4. Inter-porosity flow

The inter-porosity flow is defined by the ratio between matrix permeability and fracture permeability and an inter-porosity coefficient. Permeability is directly related to the porosity of the given system and therefore matrix permeability increases towards the platform corresponding to the porosity profile. Fracture permeability is a function of fracture density, aperture and inter-porosity coefficient. The inter-porosity flow therefore mainly depends on the type of facies and the vicinity of a fault. Inter-porosity flow is the highest for shelf facies and decreases towards the basin. For very low matrix porosities (intermediate to distal slope facies), the inter-porosity flow mostly depends on the extent of the fracture network.

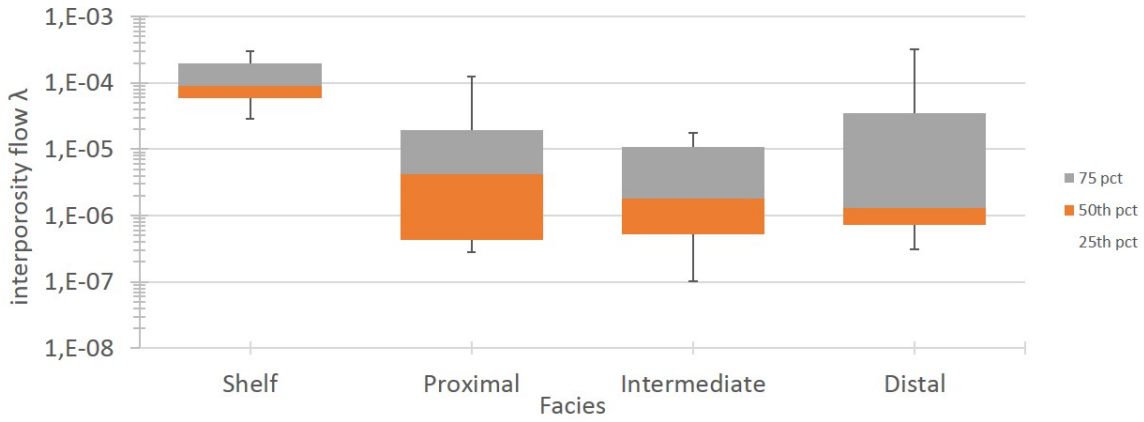

Figure 4.14: Inter-porosity flow range for specific facies. nr of wells: Shelf = 3. Proximal = 7. Intermediate = 9. Distal = 4.

4.4. Facies averaged production profiles

The fitted production profiles are given in appendix B.1. Well 7 is given as an example in figure 4.15. Main characteristics of the decline curves are high initial flow rate with a quick decline at first. After all the gas from the fracture porosity is produced, a transitional flow rate (characterized by the inter-porosity flow λ) is introduced and the flow rate remains constant for a very small amount of produced gas. After the transition from fracture production to total system production, the decline resumes approximately linear decline until all gas is produced. The modeled high initial rates often do not coincide with the initial flow rates of the given wells due to choking of a well, the inaccuracy of monthly averaged data or the model.

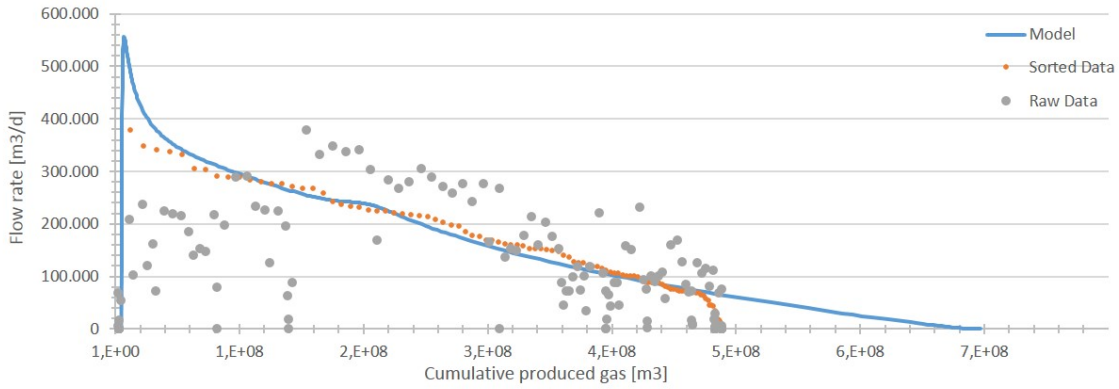

Figure 4.15: Modeled production profile for well 6.

The median values (i.e. second quartile Q2 or 50^{th} percentile) for each specific facies is used to model an average production profile for the specific facies. As can be seen in figure 4.16, proximal slope and shelf facies are considered best reservoirs with highest initial rates per meter reservoir ($16.000\ \frac{m^3}{day}$) and cumulative gas production ($9{\cdot}10^8 m^3$). Moving towards the basin initial flow rate per meter reservoir and cumulative gas production decreases to $3.500\ \frac{m^3}{day}$ and $2 \cdot 10^8 m^3$, respectively. The 25^{th} percentile (first quartile Q1) and the 75^{th} percentile (third quartile Q3) values are used to illustrate the range of production profiles for each facies. The input values for storativity ratio, inter-porosity flow, initial flow rate and dimensionless reservoir radius are given in appendix B.4.

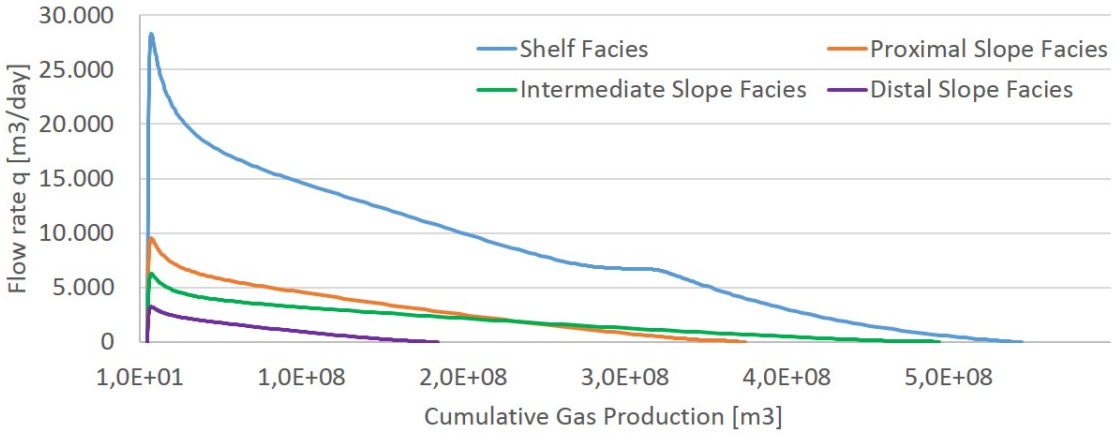

Figure 4.16: Facies averaged production profiles.

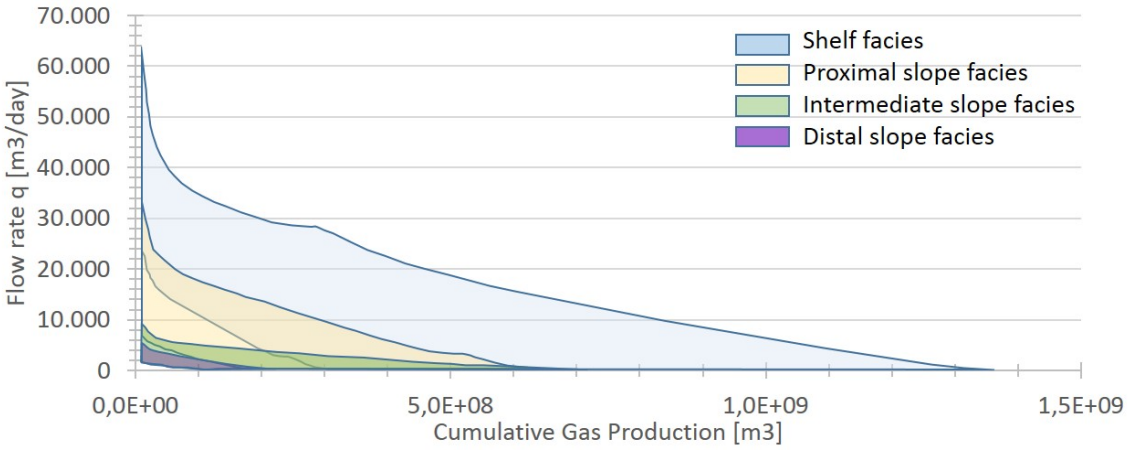

Figure 4.17: Facies production profile range between the 25^{th} percentile and 75^{th} percentile.

5

Discussion

The Warren & Root model is a highly simplified model for naturally fractured carbonate modeling. Assumptions and methods limit the studies outcome and comparability to real data. In the following chapter the quality of the data, model and assumptions are reviewed.

5.1. Quality of the data

First of all, the available production data for Zechstein-2 Carbonate Member in South-East Drenthe is monthly averaged. This gives the main implication that initial high flow rates are averaged and often lower than the true initial rate. When initial flow rates exceed surface facility limits, the wells are choked or minimum wellhead pressure is reached, flow rates can not be attributed to reservoir characteristics.

5.2. Validity of the chosen model

The Warren & Root model is valid when the matrix storage capacity is considerably larger than the fracture storativity and the matrix permeability is considerably lower than the fracture permeability.

Permeability difference The assumption that fluid flows from the matrix system into the fracture system and subsequently into the wellbore is only valid when above mentioned assumptions are true. In figure 5.1 the difference between fracture permeability and matrix permeability is depicted. Only for the first 5 wells it is doubtful whether the dual-porosity model is applicable since the difference is less than a factor 10. For all other wells it is assumed that a factor 10 is sufficient and thus the Warren & Root model can be applied. When matrix porosity becomes extremely high (i.e. shelf facies with porosity > 10%) the assumption that fluid flows from the matrix system into the fracture system and subsequently into the wellbore probably does not hold anymore, since matrix porosity is perfectly able to produce itself directly into the wellbore. Two different factors play a role in the difference between matrix permeability and fracture permeability:

- Fracture permeability is very low (i.e. almost no flow)
- Matrix permeability is very high (i.e. proximal slope to shelf facies)

If a well encounters very little fractures, the flow rates are minimal and consequently fracture permeability is low. This might be caused by the fact that a well is drilled (sub-)parallel to the fracture sets, encountering little or no fractures. If the matrix permeability is very high, the apertures of the fractures will be overestimated because all flow is assigned to fracture flow while a part of the flow should be assigned to matrix production. This is seen in figure 4.10 & 4.6. Subsequently, fracture density will be underestimated (Figure 4.9 & 4.5).

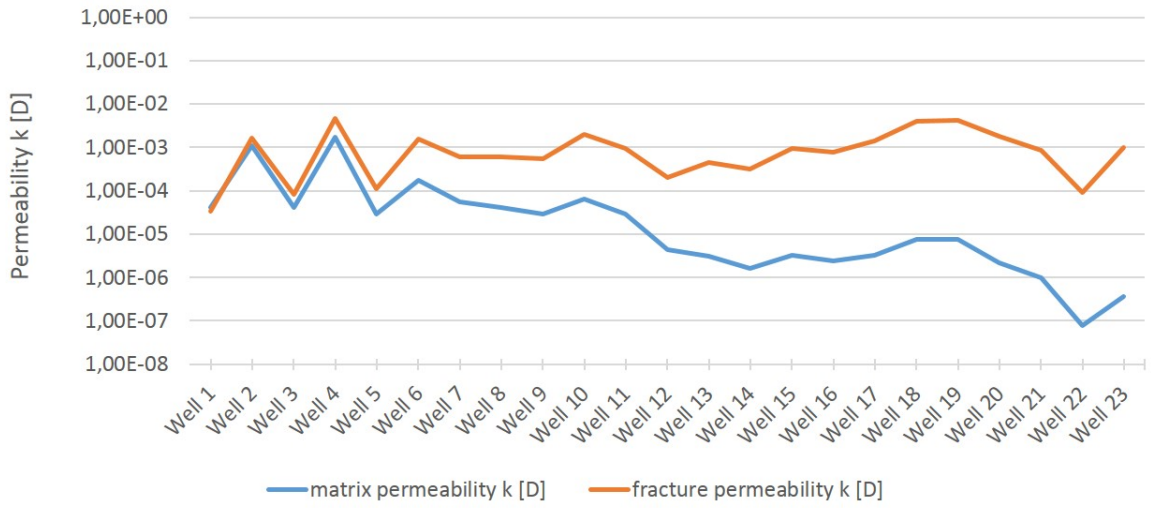

Figure 5.1: Difference between matrix permeability and fracture permeability.

Fracture density Frikken et al. stated that the fracture density of individual hairline fractures in the Drenthe area is in de order of decimeters to meters [9]. This means that fracture density ranges from 1 to 10 fractures per meter. The spacing-aperture relation depicted in figure 3.10 is chosen such that it intersects the measured values from CBIL logs on macro-fractures (apertures approximately 25-35 cm with spacings of approximately 250-500 m) and the corresponding fracture density lies within the range specified above and in figure 5.2.

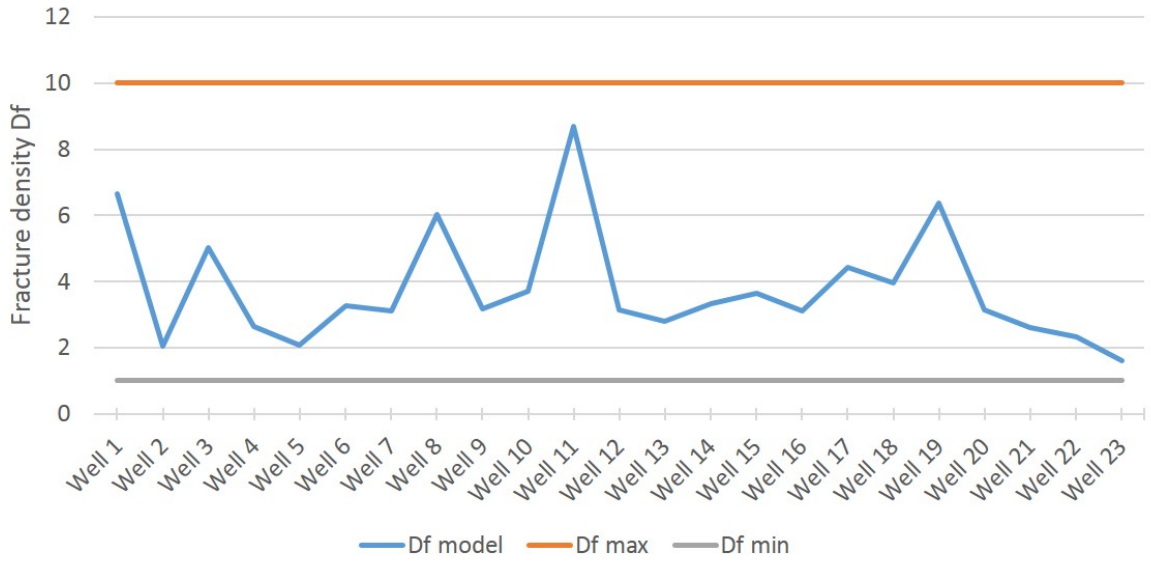

Figure 5.2: The validity of the fracture density input for the Warren & Root model. The density falls between the range given by Frikken et al..

Storativity ratio Fracture porosity is usually very small. Values between 0.0001 and 0.001 of rock volume are typical (0.01% to 0.1%). This means that, for a given matrix porosity, the range of the storativity ratio ω can be calculated and is illustrated in figure 5.3.

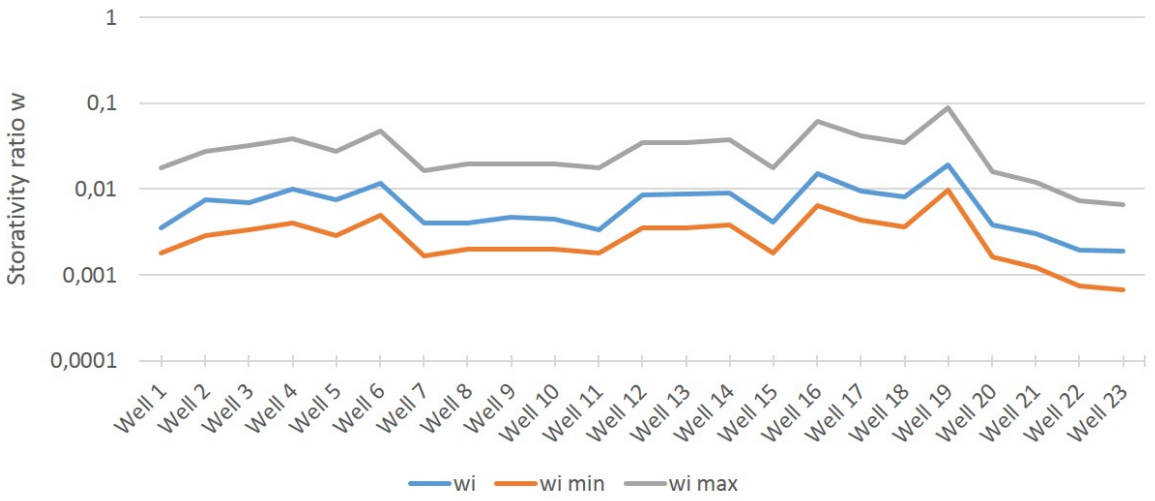

Figure 5.3: Storativity ratio ω boundaries (wi_{min} and wi_{max}) and the storativity ratio wi calculated using the Warren & Root model.

5.3. Core fracture analysis

To support the Warren & Root fracture aperture and density input parameters, a core fracture analysis is carried out. Five wells were selected with varying characteristics facies and initial production rate. In addition, the wells were chosen where the cored interval coincide with the perforated interval to enable the possibility to calculate true fracture density for the whole producing interval. The core fracture analysis show similar densities for Emmen-12 and Oosterhesselen-02 but much too low densities for the other two wells (figure 5.4). This could be due to two main reasons: The Warren & Root model assumes high densities with very small apertures for these two wells, the apertures are so small that fractures were under-sampled in the core analysis. Another possibility is that the encountered fracture density for the Emmen-12 well and Oosterhesselen-02 is very low due to the direction the well has been drilled. Little is known on fracture orientation and the core orientation is not known. A correction for encountered fracture density is applied to obtain true fracture density but this method is very inaccurate and might not be executed correctly.

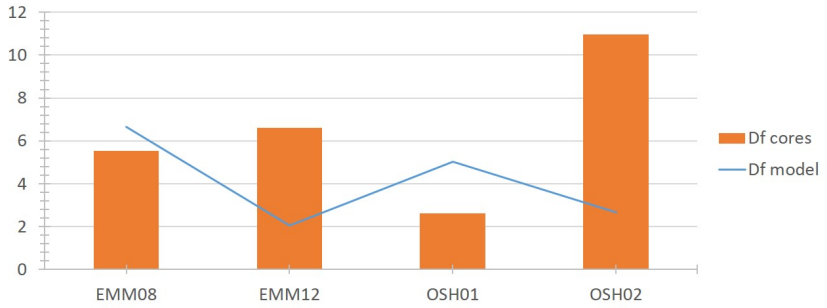

Figure 5.4: Comparison between core fracture density and model fracture density

5.3.1. Fracture dip & orientation

The preferred drilling direction is perpendicular to the horizontal principal stress (e.g. EW trending (sub-)horizontal) to encounter the highest fracture density. The encountered fracture density is therefore a function of the drilling direction and is not always comparable to the true fracture density. The wells in this area show a variation in drilling directions and should therefore be corrected to obtain the encountered fracture density. This difference is corrected using the encountered fracture density from the core fracture analysis and the probability of encountering the specified fracture sets as a function of drilling direction. The fractured core analysis was conducted on five different wells with different characteristics. All cores were slabbed because the operator has to provide parts of the cores to TNO

and none of the cores were oriented. This led to the complication that all fracture dips were apparent dips and no conclusion could be made on true fracture orientation in space. Stylolith occurrence was also recorded and showed that all styloliths were parallel to bedding. This implies that the styloliths from all cores belonged to the same oriented stress field, and could therefore be used in combination with the well orientation to calculate slabbed core orientation and subsequently true fracture orientation. First, the orientation of each well at Zechstein-2 Carbonate Member level was plotted in a stereo-plot. The average measured dip of the styloliths of each well was then plotted as a circle around the wells orientation. This circle represents all possible true dip orientations of the measured styloliths within each well (figure A.4). The intersection of all circles represents the only solution for the stylolith true orientation. Stylolith orientation is then used to plot the slabbed core orientation in the stereo-plot. Apparent measured fracture dip is then plotted on the slabbes core orientation lines for each well (Figure A.5). Apparent fracture dips are normalized using histograms. The prevailing principal stress is N-S oriented resulting in NS oriented extensional fractures, and a conjugate set of Riedel shear fractures with orientations 340° and 20° with calculated corresponding dips.

5.3.2. True fracture density

The true fracture density is a function of the orientation of the scanline (i.e. borehole) with respect to the fractures orientation. True fracture density is found when the fracture set is perpendicular to the scanline (figure 5.5). Therefore, the true fracture density can be calculated using the following formula which assigns value 1 to drilling perpendicular to the fracture set and 0 when drilled parallel to the fracture set:

$$Truefracturedensity D_f = \frac{NF * D_{f,e}}{\sum_{i=1}^{NF} cos(\theta_{1,i}) * cos(\theta_{2,i})} \tag{5.1}$$

$$Openfracturedensity D_f = \frac{\sum_{j=1}^{NF-1} NF * cos(\theta_{1,j}) * cos(\theta_{2,j}) * D_{f,e}}{\sum_{i=1}^{NF} cos(\theta_{1,i}) * cos(\theta_{2,i})} \tag{5.2}$$

where;
$NF = \#offracturesets(NF = 3)$
$D_{f,e} = EncounteredFractureDensity$
$\theta_1 = |cos(90 - \theta_{drillingdip} - \theta_{fracturesetdip})|$
$\theta_2 = |cos(\theta_{drillingorientation} - \theta_{fracturesetorientation})|$

i = 1,2 and j = 1,2,3 representing fracture set 1,2 and 3 (i.e. R', E and R, respectively).[1] The sensitivity is studied by varying the assumed fracture set orientation with varying principal stress from NS-oriented to NW-SE oriented and fracture set dips are varied by obtained standard deviation to obtain minimum and maximum possible percentage open fractures of the total fracture density.

Figure 5.5: Effect of scanline orientation with respect to fracture set. Scanline perpendicular to fracture set; # fractures = 12, scanline 45° to fracture set; # fractures = 10.

[1] As previous studies have shown that fracture sets E and R' are open fractures while fracture set R is closed [9]; only the first-mentioned sets (i.e. E and R') are considered as sets enhancing gas flow.

6

Conclusions

The following conclusions can be made from this study:

Warren & Root dual porosity model

- The Warren & Root model is an applicable model for the Zechstein-2 Carbonate Member naturally fractured carbonate reservoirs and shows reasonable comparable production profiles on the analyzed wells despite many simplifying assumptions.

Fracture networks

- The fracture network is the most important parameter for distal- to proximal slope facies. Fractures must be present since matrix porosity and permeability is too low for sustainable production.
- Fracture aperture is the main controlling parameter on fracture porosity and therefore on fracture permeability.
- Distance to the nearest open fault is highly important. Flow rates increase for distal- to proximal slope facies further away from the fault. Shelf facies flow rate increases towards an open fault zone. This is probably due to differences in configuration of open fault zones in low porosity and high porosity host rocks.
- Shelf facies productivity is mostly dependent on matrix porosity.

Matrix porosity

- Matrix porosity increases towards the platform fringe and increases the possibility of larger connected gas volumes.

Facies productivity

- Initial flow rate is a good indicator for connected gas volume, but can not be linearly extrapolated.
- Well productivity decreases from shelf facies towards the basin.
- Shelf facies have high average initial flow rates of $27.000\ \frac{m^3}{day}$ per meter reservoir and average cumulative gas production of $9 \cdot 10^8\ m^3$. The average initial flow rate of distal slope facies only reaches values of $3.500\ \frac{m^3}{day}$ per meter reservoir and average cumulative gas production is approximately $2 \cdot 10^8 m^3$.

General

- The present-day principal stress in the Drenthe province is mainly parallel to the extensional open fracture trend and has probably contributed to their preservation. Consequently, knowledge on structural deformation history and present-day stress fields are compulsory for field development of low porosity carbonates.
- Wells should be drilled perpendicular to the maximum principle stress to encounter the highest fracture density. In this case this means drilling east-to-west or west-to-east and preferably horizontal.
- Most Zechstein-2 Carbonate Member wells show a very high initial rate, fast decline and a moderate linear decline until the well is killed or exhausted.

7

Recommendations

Zechstein-2 Carbonate Member prospects Several new promising prospects have been identified around the Elbow Spit High and other areas. In the Drenthe area, fracture networks are majorly important for the productivity of a well. For future drilling programs, it is highly important to understand the structural deformation history and present-day principle stress of the area. This gives an insight in the orientation of the possibly present open fracture networks. Although the porosity trend of carbonate reservoirs normally increases towards platform facies, diagenesis and depositional environments can influence porosity and might vary along the Southern Permian basin margin. Direct extrapolation of this study to other areas is therefore not recommendable and care should be taken. This study is only intended to give extra insight on general behavior of carbonate reservoirs and to highlight important reservoir parameters to decrease the uncertainty of future drilling programs.

A

Appendix A

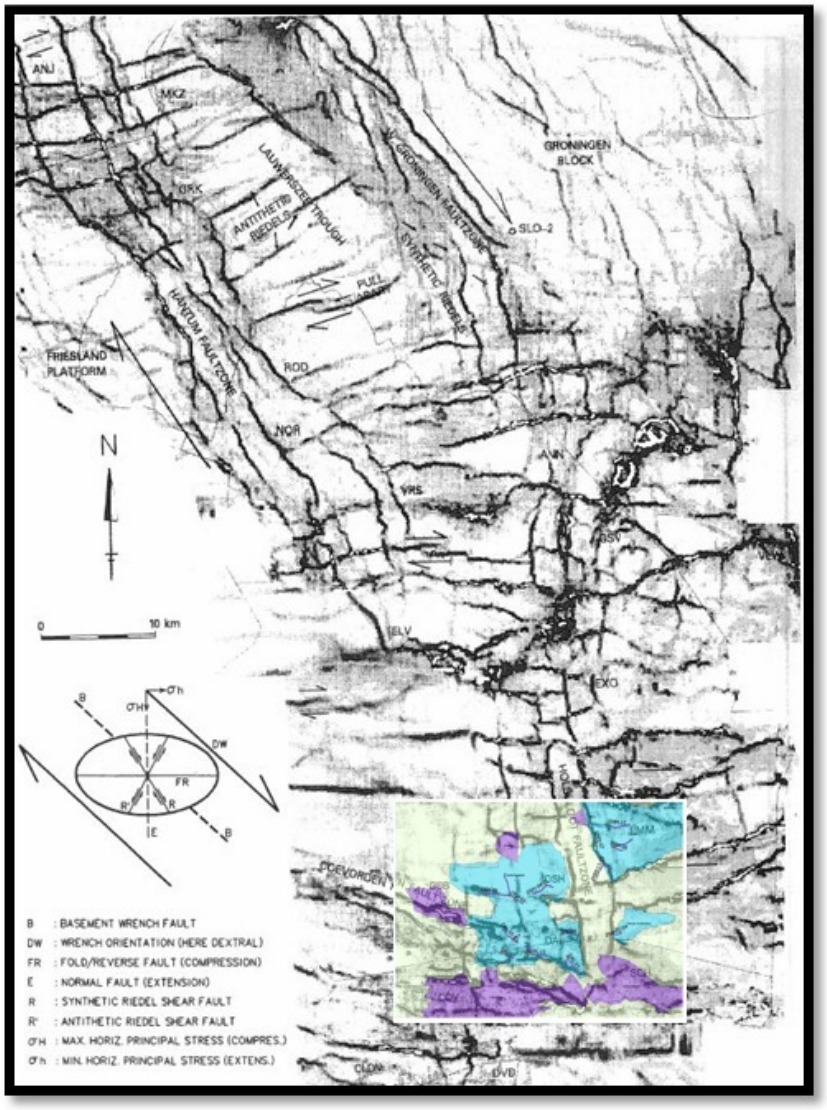

Figure A.1: Dip-map of top Zechstein-2 Carbonate Member. En-echelon left-stepping Riedel faults, pull-apart basins and rhomboidal fault patterns are characteristic features of dextral wrenching. [9]

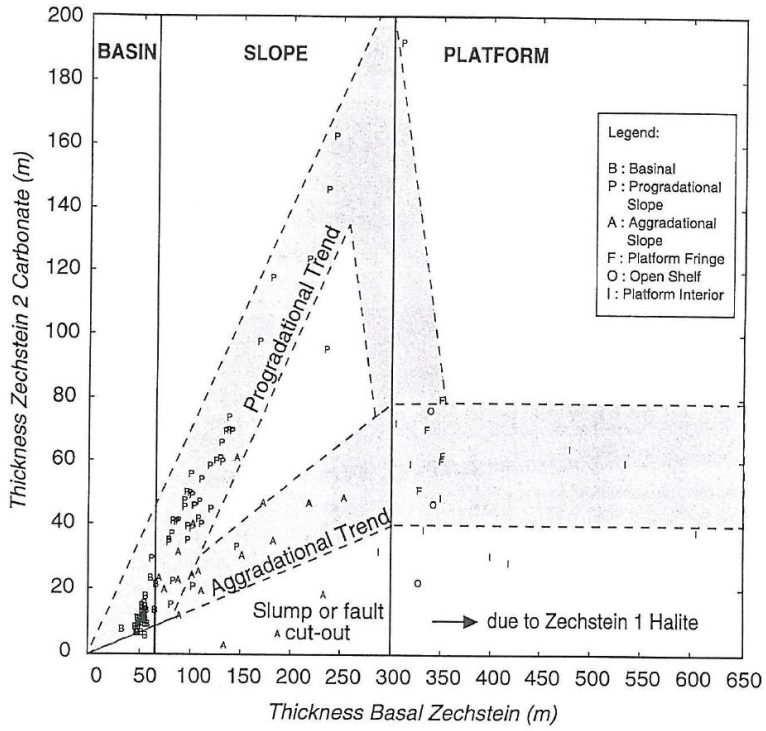

Figure A.2: Graph showing the thickness relationship between the Zechstein-2 Carbonate Member and the Basal Zechstein Unit found in wells in the NE Netherlands.

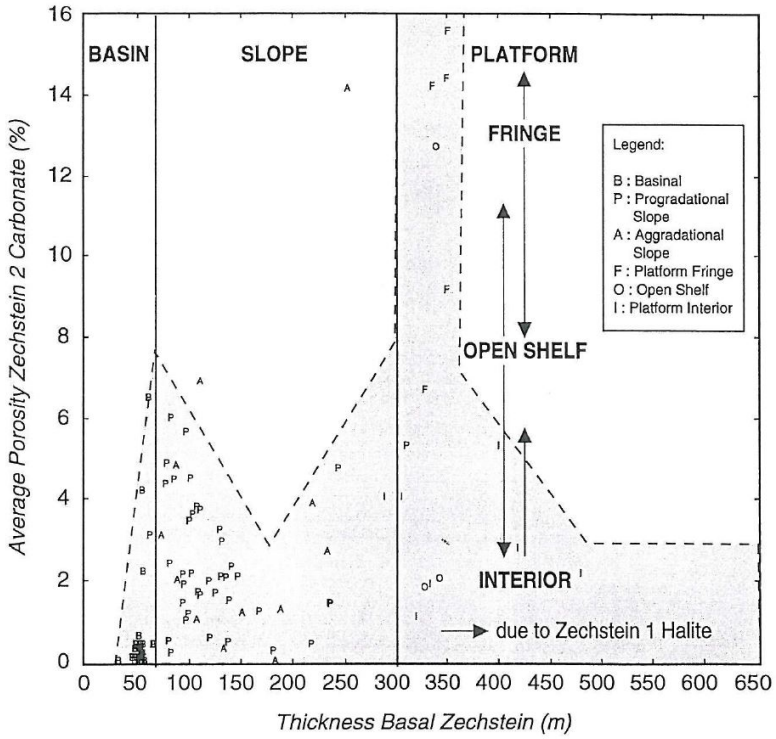

Figure A.3: Graph showing the relationship between the average porosity in the Zechstein-2 Carbonate Member in wells in the NE Netherlands.

WELL	median ☐[%]	median k [mD]
DALEN-2A	2.1	0.7
DALEN-09B	2.1	0.12
DALEN-01-1	0.9	0.005
DEN VELDE-03-1	2.6	0.01
EMMEN-08	0.4	0.03
EMMEN-12	4.0	0.03
EMMEN-7	0.5	0.03
EMMEN-NIEUW-AMSTERDAM-01B	1.7	0.03
GASSELTERNIJVEEN-01B	16.35	2.59
HOOGENWEG-01	9.3	1.52
OLDELAMER-01	13.55	4.05
OLDELAMER-02	9.1	0.68
OOSTERHESSELEN-01	1.4	0.03
OOSTERHESSELEN-02	1.2	0.03

Table A.1: Table showing all core measurements within the area of interest used for this analysis, porosity and permeability are medians of each dataset.

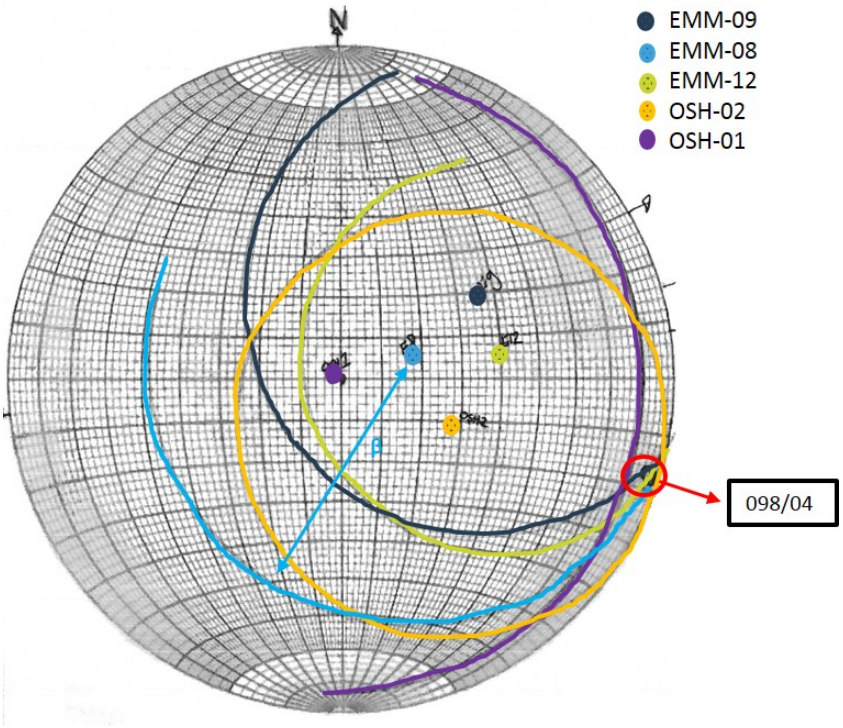

Figure A.4: Stereoplot showing true stylolith orientation and dip using apparent dips from 5 different wells (coloured dots).

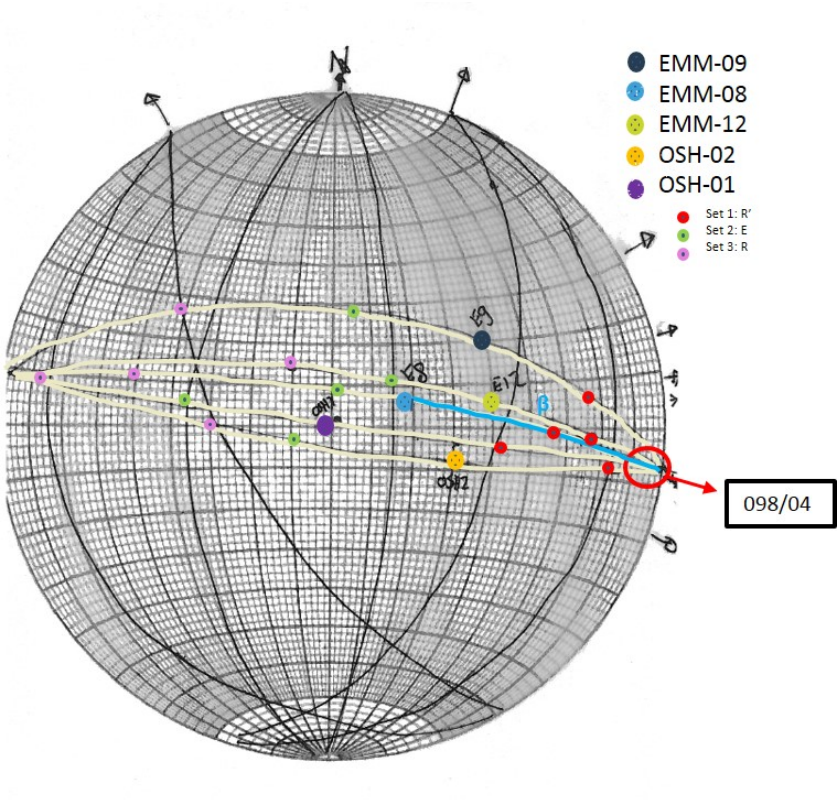

Figure A.5: Stereoplot showing true stylolith orientation and dip using apparent dips from 5 different wells. white lines: slabbed core orientation. black lines: implied NS-oriented fracture orientation with corresponding conjugate fractures.

WELL	Cum. Gas Production $N_P[m^3]$	Reservoir Radius R_e	Skin effect [-]	Dim. Reservoir Radius R_{eD} [-]
Well 1	$2.69 \cdot 10^7$	106	-4.69	11
Well 2	$2.53 \cdot 10^8$	769	-5.31	43
Well 3	$9.47 \cdot 10^9$	459	-5.40	23
Well 4	$4.58 \cdot 10^8$	1087	-5.30	61
Well 5	$1.04 \cdot 10^8$	1184	-4.88	101
Well 6	$4.89 \cdot 10^7$	727	-4.86	64
Well 7	$4.03 \cdot 10^8$	545	-4.68	57
Well 8	$5.41 \cdot 10^8$	312	-5.35	17
Well 9	$4.16 \cdot 10^7$	698	-4.91	58
Well 10	$1.98 \cdot 10^8$	481	-4.99	37
Well 11	$2.04 \cdot 10^8$	183	-5.41	9
Well 12	$1.10 \cdot 10^8$	582	-5.54	26
Well 13	$1.71 \cdot 10^8$	725	-5.49	34
Well 14	$5.53 \cdot 10^8$	843	-4.93	69
Well 15	$8.35 \cdot 10^8$	1036	-4.88	88
Well 16	$2.08 \cdot 10^8$	568	-5.13	38
Well 17	$8.62 \cdot 10^8$	891	-4.71	90
Well 18	$1.93 \cdot 10^8$	504	-5.06	36
Well 19	$1.77 \cdot 10^8$	467	-5.03	34
Well 20	$3.58 \cdot 10^8$	663	-4.95	53
Well 21	$2.76 \cdot 10^7$	160	-5.09	11
Well 22	$4.18 \cdot 10^7$	244	-5.26	14
Well 23	$1.07 \cdot 10^8$	389	-5.16	25
Well 24	$1.75 \cdot 10^9$	425	-3.54	138
Well 25	$1.07 \cdot 10^8$	261	-4.76	25
Well 25	$4.58 \cdot 10^8$	582	-4.67	61

Table A.2: Reservoir radius, dimensionless reservoir radius and skin effect for analyzed wells.

B

Appendix B

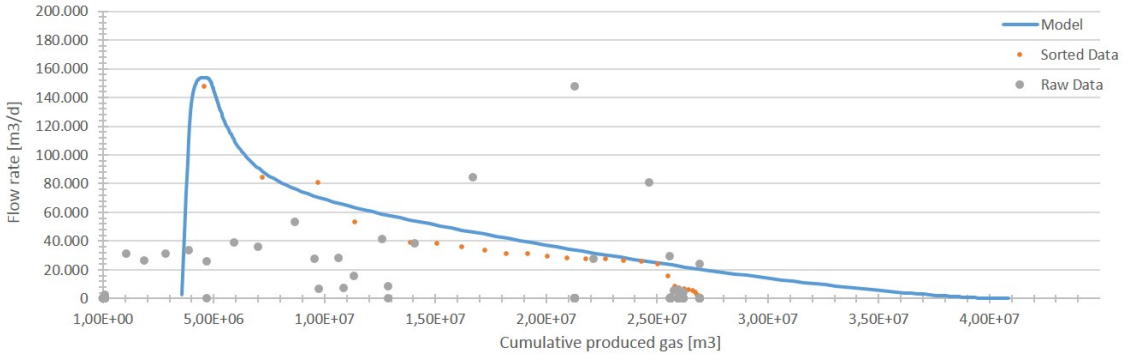

Figure B.1: Production profile Well 1

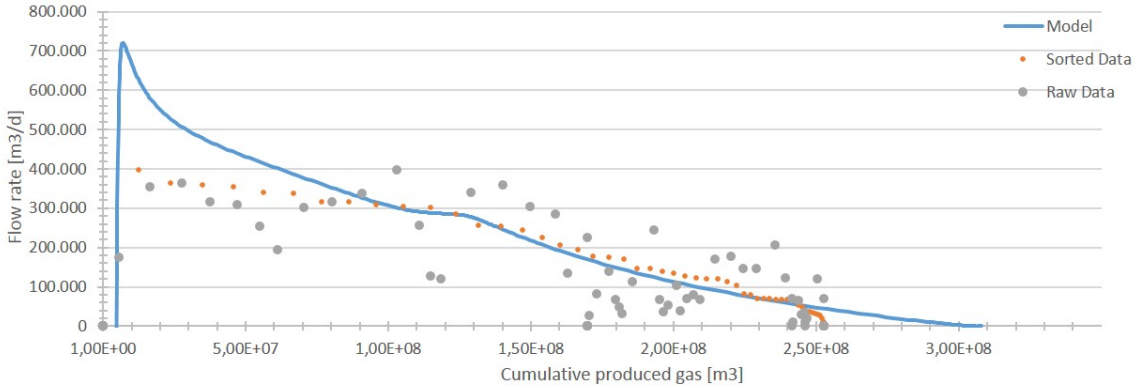

Figure B.2: Production profile Well 2

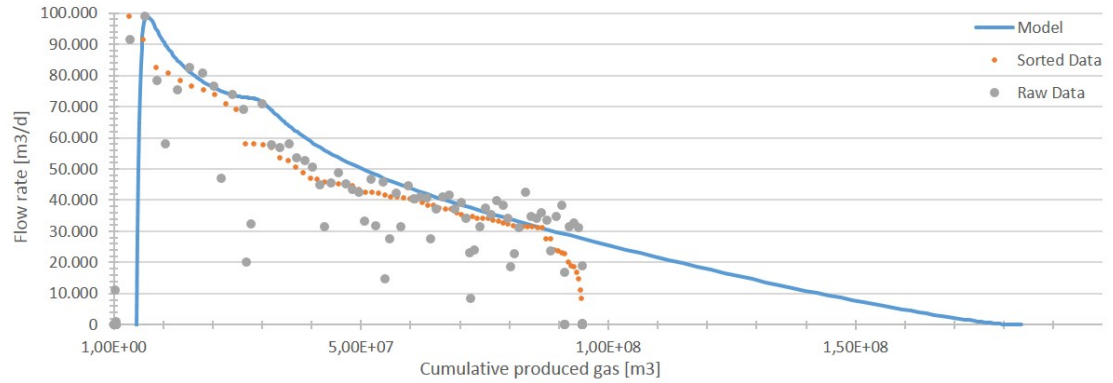

Figure B.3: Production profile Well 3

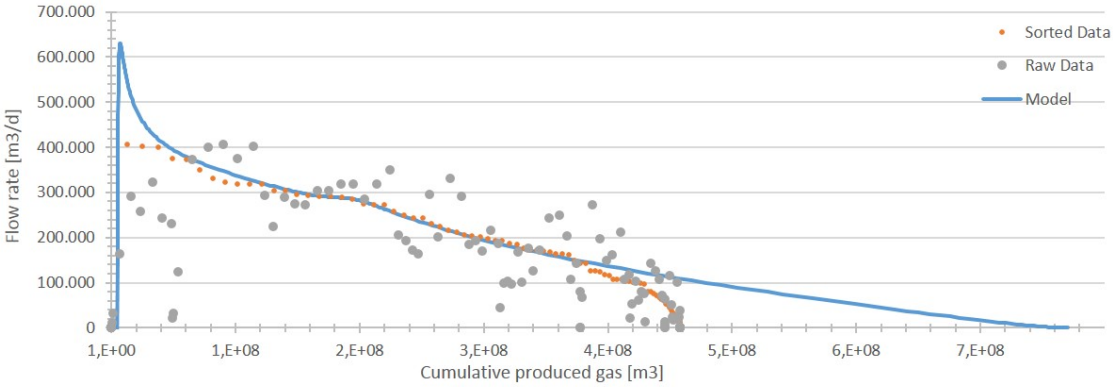

Figure B.4: Production profile Well 4

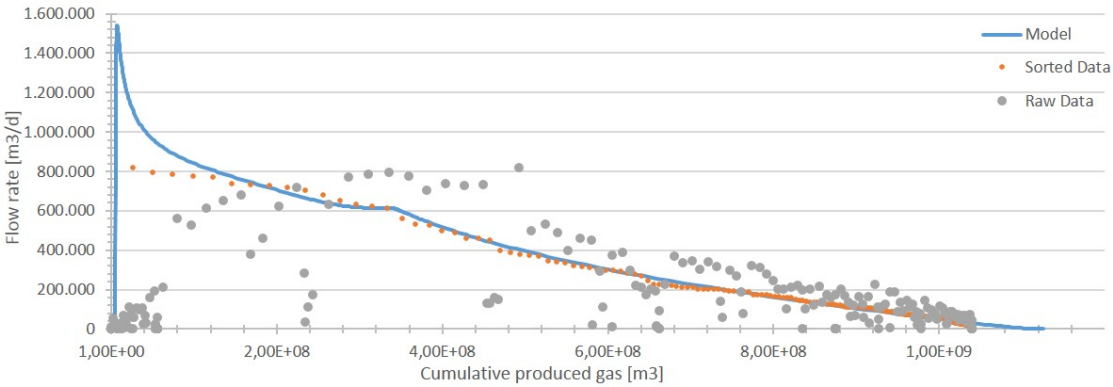

Figure B.5: Production profile Well 5

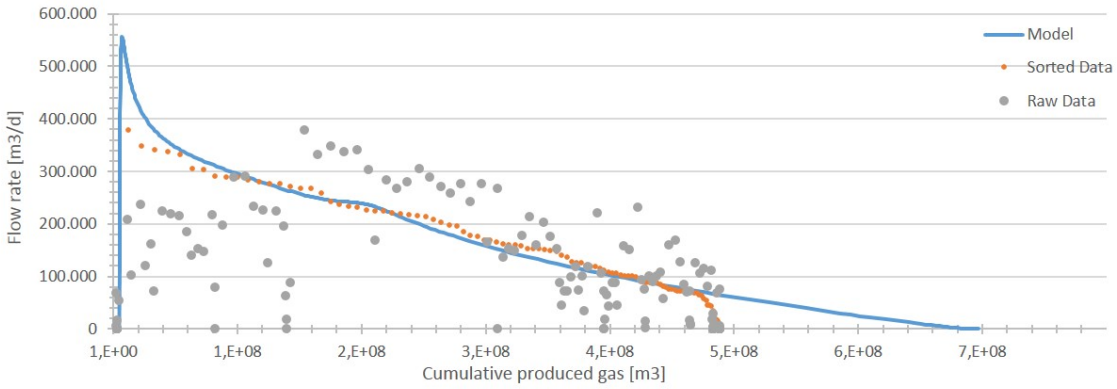

Figure B.6: Production profile Well 6

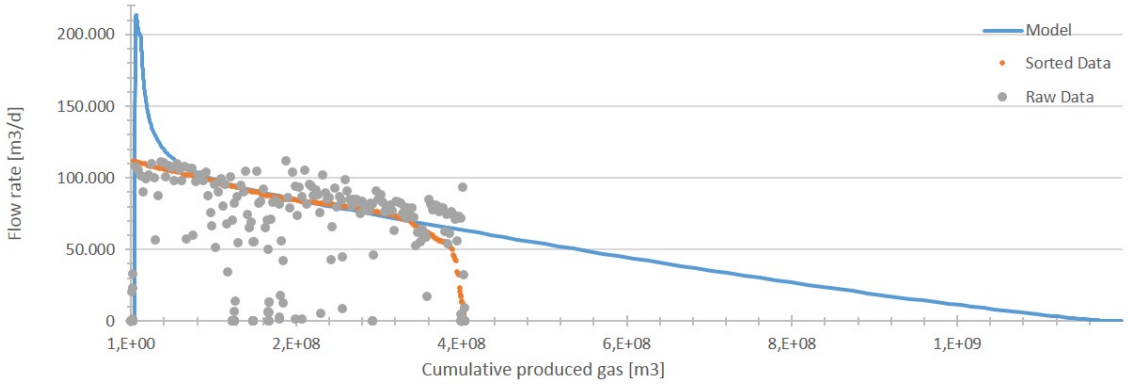

Figure B.7: Production profile Well 7

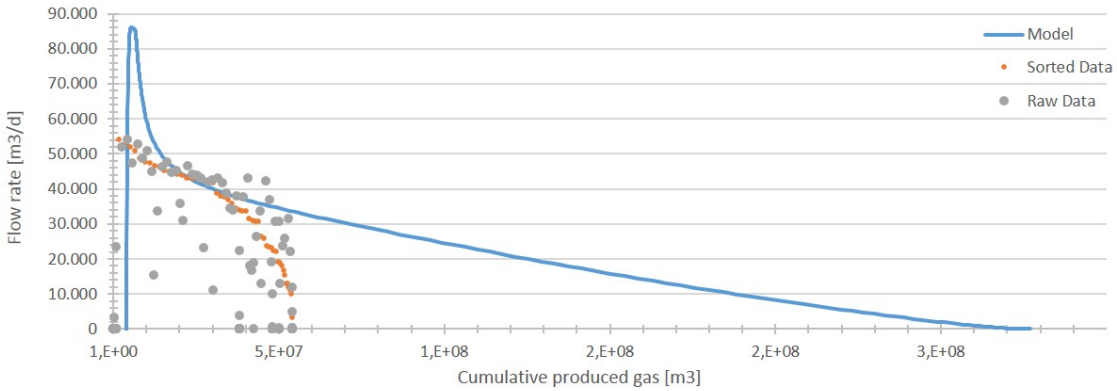

Figure B.8: Production profile Well 8

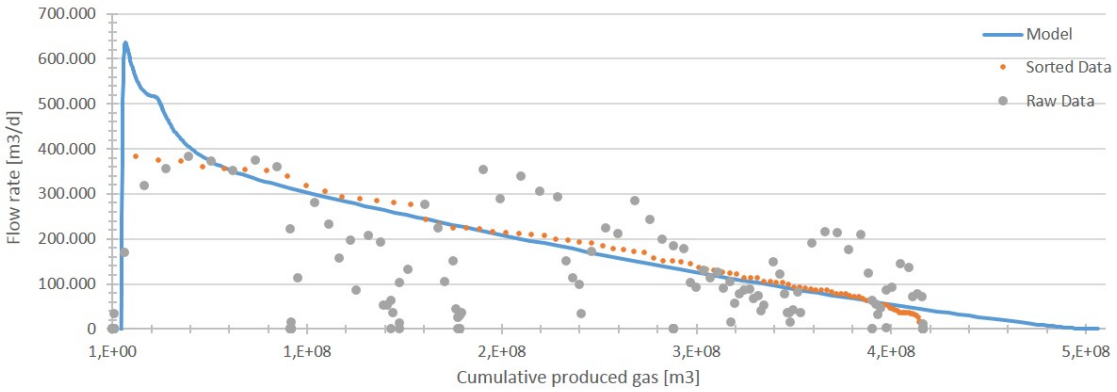

Figure B.9: Production profile Well 9

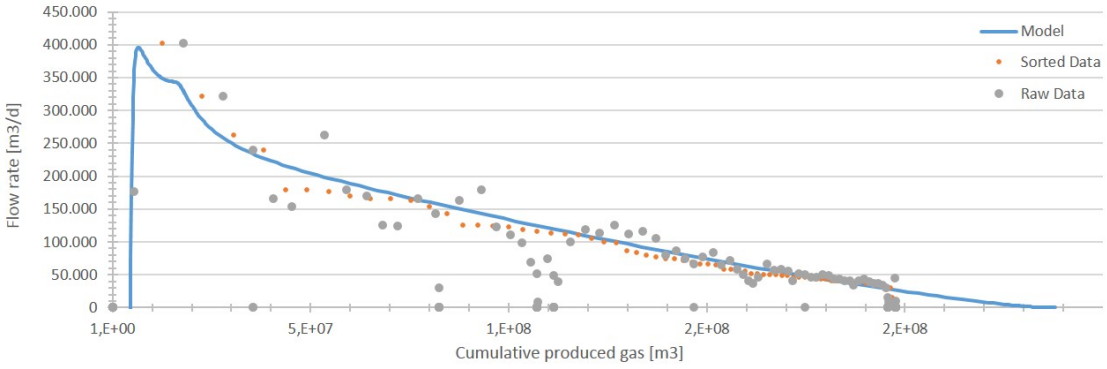

Figure B.10: Production profile Well 10

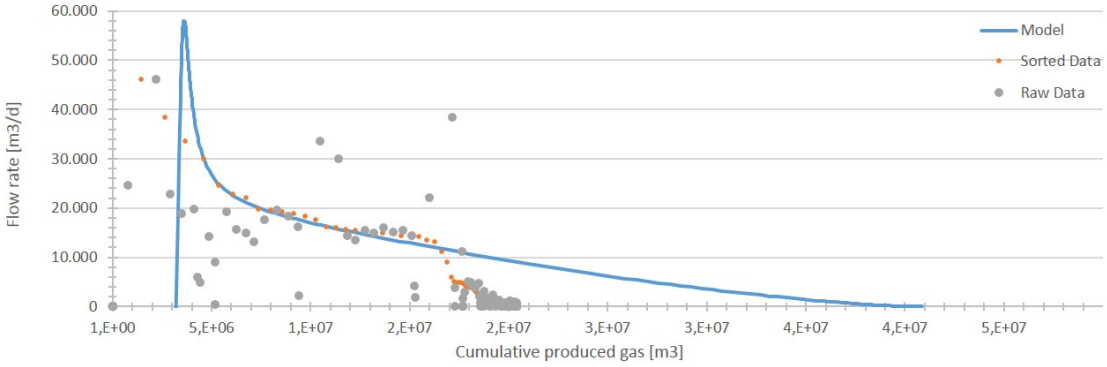

Figure B.11: Production profile Well 11

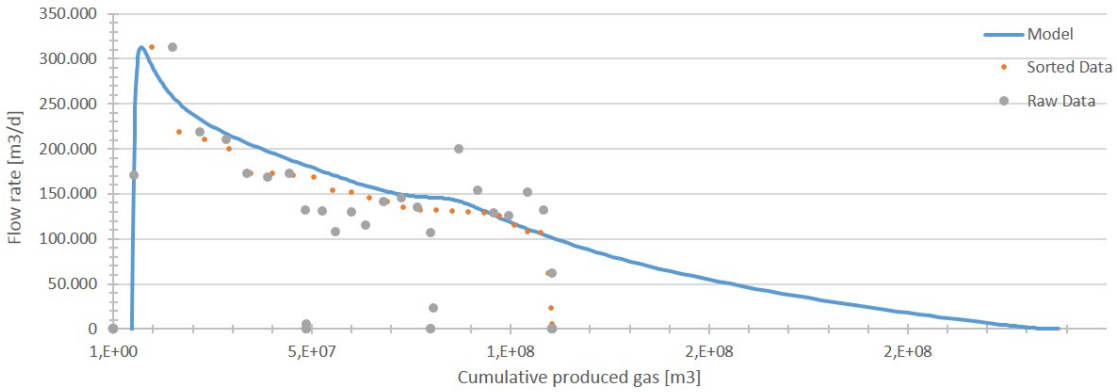

Figure B.12: Production profile Well 12

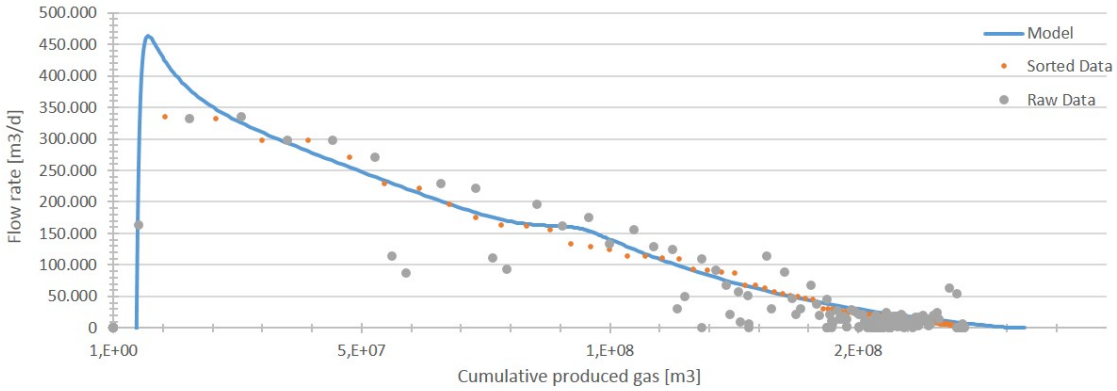

Figure B.13: Production profile Well 13

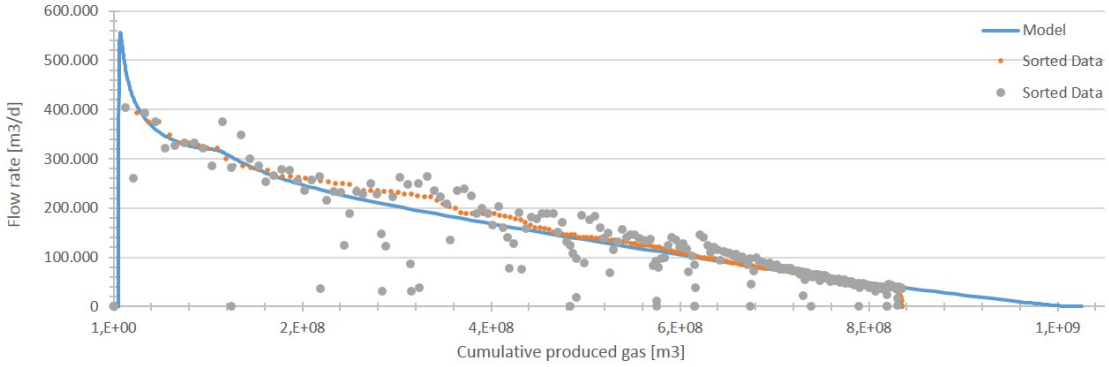

Figure B.14: Production profile Well 14

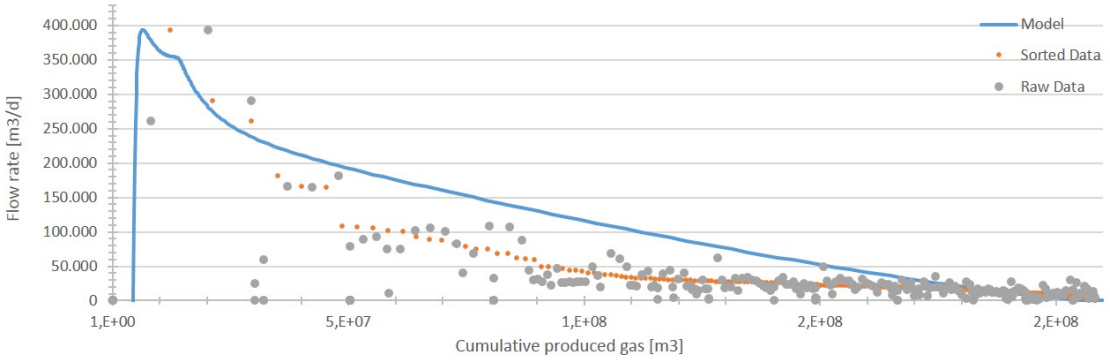

Figure B.15: Production profile Well 15

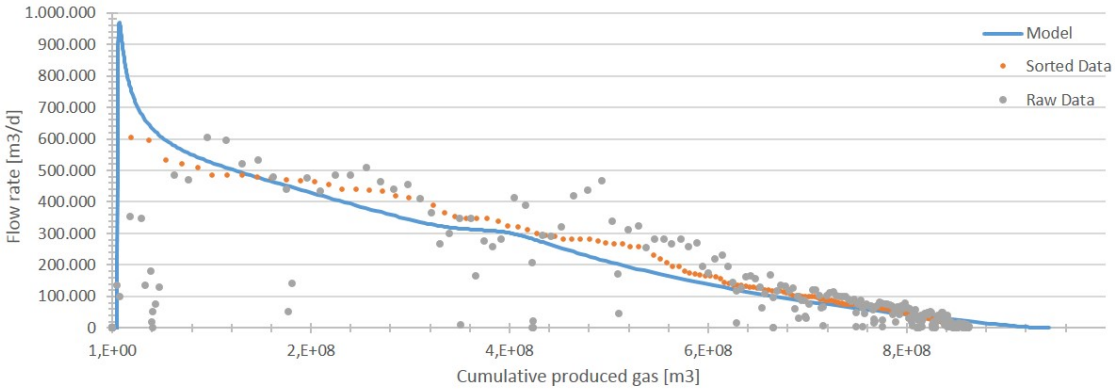

Figure B.16: Production profile Well 16

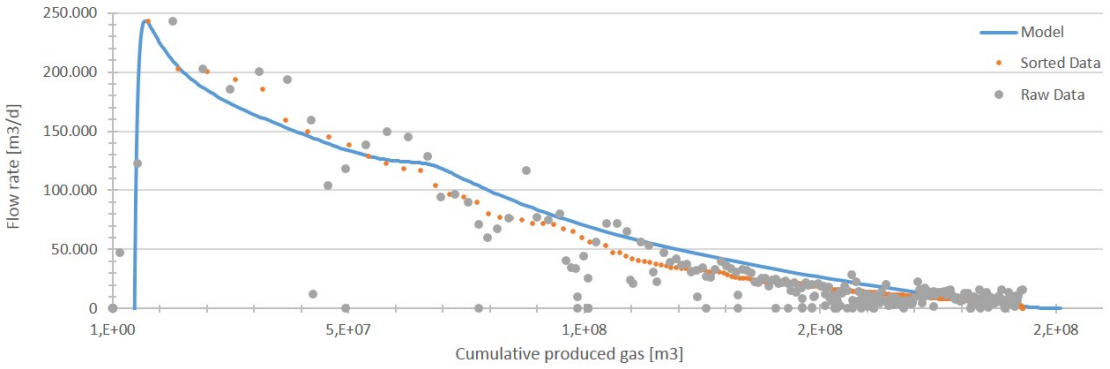

Figure B.17: Production profile Well 17

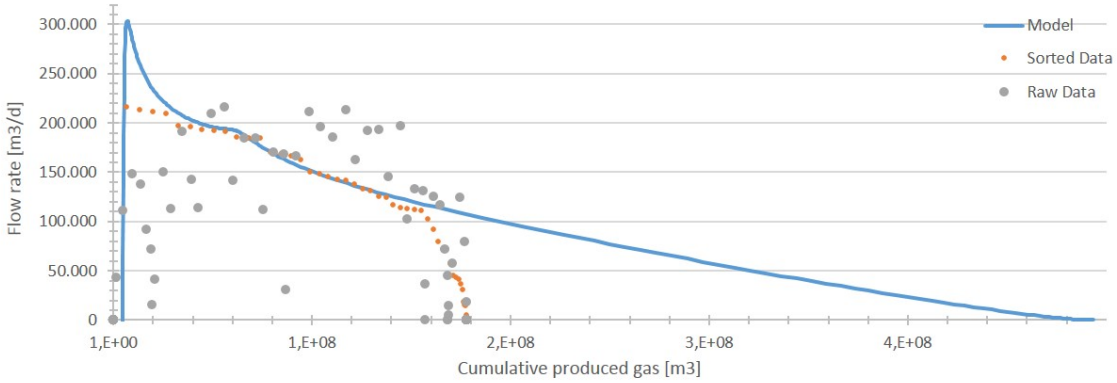

Figure B.18: Production profile Well 18

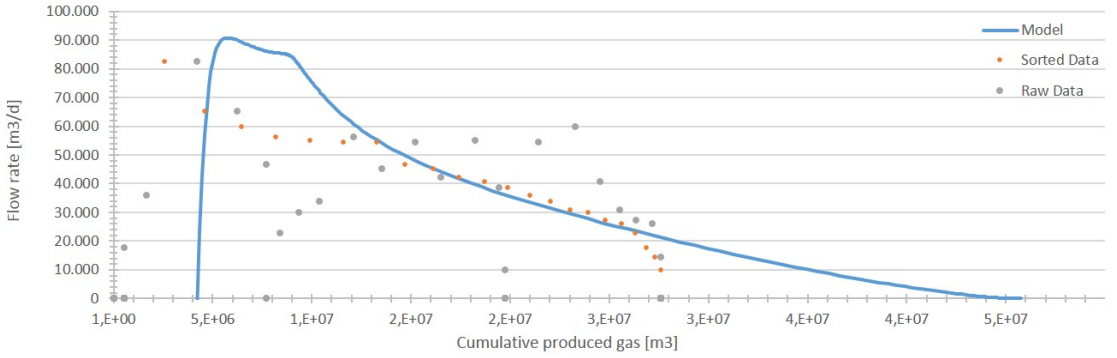

Figure B.19: Production profile Well 19

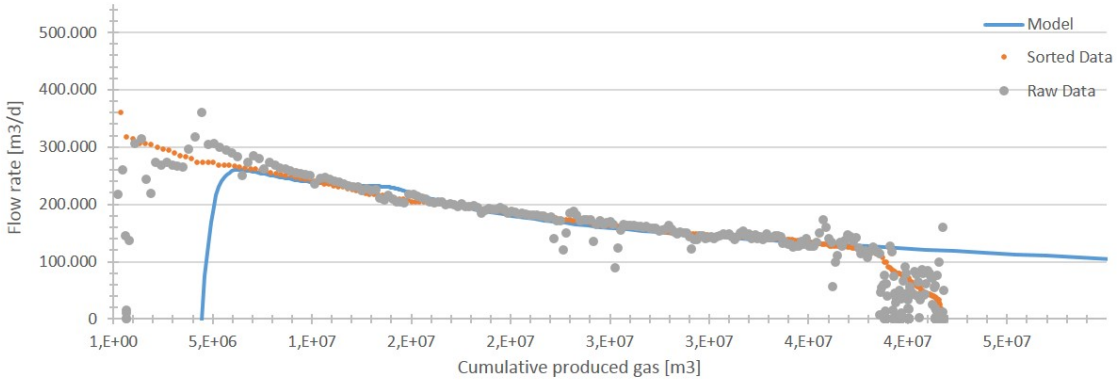

Figure B.20: Production profile Well 20

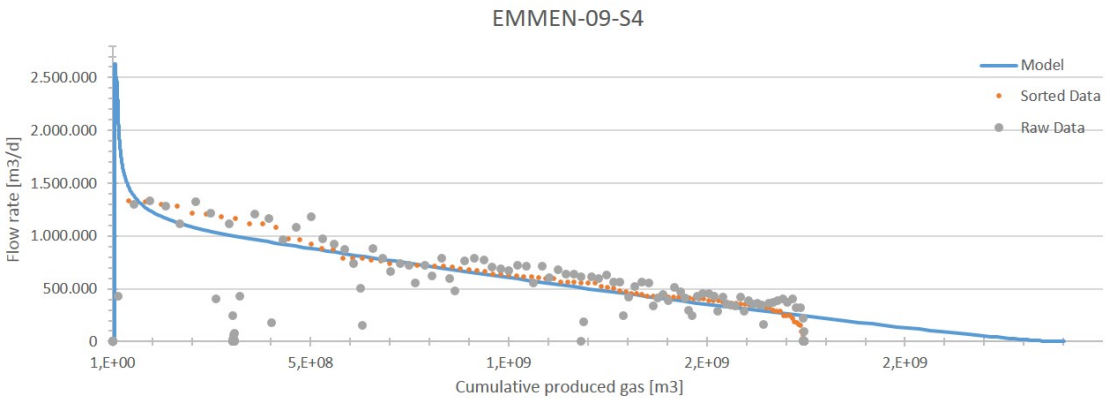

Figure B.21: Production profile Well 21

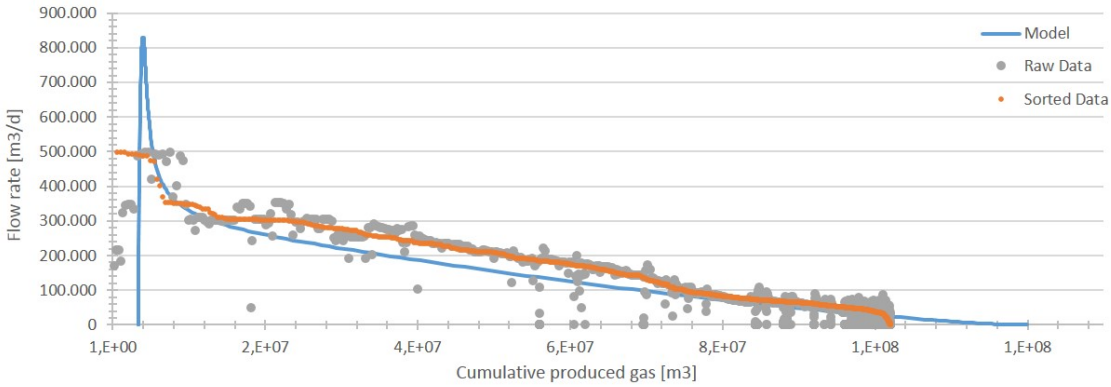

Figure B.22: Production profile Well 22

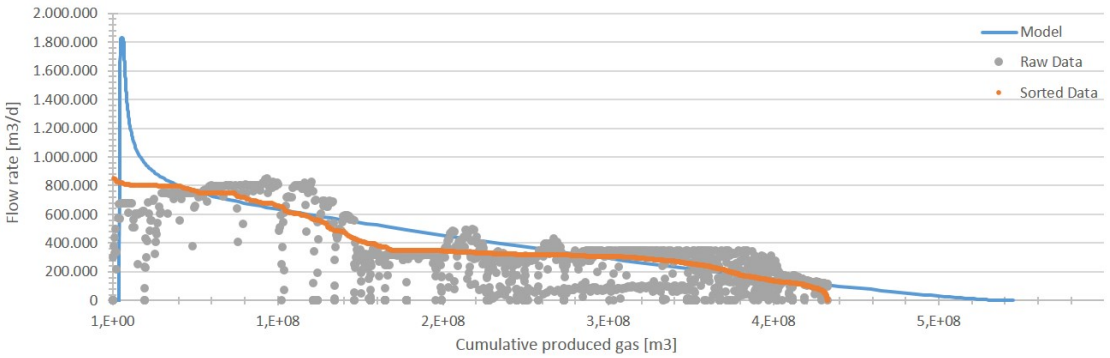

Figure B.23: Production profile Well 23

Table B.1: Storativity ratio values for each specific facies

Storativity ratio	**Shelf**	**Proximal**	**Intermediate**	**Distal**
Average	2,28E-03	6,31E-03	9,30E-03	7,28E-03
Min	1,87E-03	3,56E-03	4,14E-03	3,35E-03
Q1	1,90E-03	3,83E-03	4,60E-03	5,54E-03
Median	1,92E-03	5,67E-03	8,13E-03	8,46E-03
Q3	2,49E-03	7,52E-03	1,22E-02	9,10E-03
Max	3,05E-03	1,16E-02	1,92E-02	9,87E-03
25th pct	1,90E-03	3,83E-03	4,60E-03	5,54E-03
50th pct	2,43E-05	1,85E-03	3,53E-03	2,92E-03
75 pct	5,64E-04	1,85E-03	4,04E-03	6,41E-04
min	2,43E-05	2,70E-04	4,61E-04	2,19E-03
max	5,64E-04	4,10E-03	7,07E-03	7,75E-04

Table B.2: Inter-porosity flow values for each specific facies

Inter-porosity flow	**Shelf**	**Proximal**	**Intermediate**	**Distal**
Average	1,40E-04	2,61E-05	6,02E-06	5,60E-05
Min	2,89E-05	2,84E-07	1,03E-07	3,12E-07
Q1	5,92E-05	4,34E-07	5,16E-07	7,34E-07
Median	8,95E-05	4,24E-06	1,80E-06	1,29E-06
Q3	1,96E-04	1,97E-05	1,08E-05	3,45E-05
Max	3,02E-04	1,24E-04	1,75E-05	3,20E-04
25th pct	5,92E-05	4,34E-07	5,16E-07	7,34E-07
50th pct	3,03E-05	3,81E-06	1,28E-06	5,60E-07
75 pct	1,06E-04	1,54E-05	9,03E-06	3,32E-05
min	3,03E-05	1,49E-07	4,14E-07	4,23E-07
max	1,06E-04	1,04E-04	6,71E-06	2,85E-04

Table B.3: Dimensionless reservoir radius values for each specific facies

Dimensionless reservoir radius	**Shelf**	**Proximal**	**Intermediate**	**Distal**
Average	87,7	56	59,7	37,7
Min	27	14	15	14
Q1	47,5	33,75	39,5	26,5
Median	68	54	64	35
Q3	118	75	80	39
Max	168	105	100	84
25th pct	47,5	33,75	39,5	26,5
50th pct	20,5	20,25	24,5	8,5
75 pct	50	21	16	4
min	20,5	19,75	24,5	12,5
max	50	30	20	45

Table B.4: Initial flow rate values for each specific facies

Initial flow rate q $\frac{m^3}{day}$	**Shelf**	**Proximal**	**Intermediate**	**Distal**
Average	49559	19378,78	6716	7164,857
Min	22283	1523	1130	953
Q1	26625	9211,085	5393	1901
Median	30967	11262,5	6851	3157
Q3	63197	33835,92	9076	12118,5
Max	95427	42337	10093	18005
25th pct	26625	9211,085	5393	1901
50th pct	4342	2051,415	1458	1256
75 pct	32230	22573,42	2225	8961,5
min	4342	7688,085	4263	948
max	32230	8501,083	1017	5886,5

Bibliography

[1] M. Geluk, *Late permian (zechstein) carbonate-facies maps, the netherlands,* Geologie en Mijnbouw/Netherlands Journal of Geosciences **79–1**, 17 (2000).

[2] E.B.N., *Zechstein carbonate prospects,* Database.

[3] S. Tolsma, *Seismic characterization of the zechstein carbonates in the dutch northern offshore,* Energie Beheer Nederland (2014).

[4] T. Reijers, *Sedimentology and diagenesis as 'hydrocarbon exploration tools' in the late permian zechstein-2 carbonate member (ne netherlands),* Geologos **18–3**, 163 (2012).

[5] P. Ziegler, *Geological Atlas of Western and Central Europe* (Shell Internat. Petroleum Mij., 1990).

[6] M. Zareenejad, *Application of decline analysis in fractured reservoirs, field case studies,* Journal of Chemical and Petroleum Engineering, University of Tehran **46**, 53 (2012).

[7] D. Van der Baan, *Zechstein reservoirs in the netherlands.* Geological Society Special Publication **50–1**, 379 (1990).

[8] T. C. N. Van der Sande, J.M.M.; Reijers, *Multidisciplinary exploration strategy in the northeast netherlands zechstein 2 carbonate play, guided by 3d seismic,* Kluwer Academic Publishers , 125 (1996).

[9] H. Frikken, *Reservoir-geological aspects of productivity and connectivity of gasfields in the netherlands,* thesis Delft University of Technology (1999).

[10] R. Nie, *Dual porosity and dual permeability modeling of horizontal well in naturally fractured reservoir,* State Key Laboratory of Oil Gas Reservoir Geology and Exploitation , 213 (2010).

[11] Wikipedia, *Wikipedia superposition principle,* (2016).

[12] G. Da Prat, *Welltest analysis for naturally-fractured reservoirs,* Stanford Geothermal Program (1981).

[13] P. Johnson, *The relation between radius of drainage and cumulative production,* SPE (1987).

[14] O. Ortega et al., *A scale-independant approach to fractgure intensity and average spacing measurements.* AAPG bulletin **90–2**, 193 (2006).

[15] J. Long, *Integrated zechstein study: Fracture analysis report,* Geospatial Research Limited (2016).

[16] L. Pomar, *Types of carbonate platforms: A genetic approach,* SPE (2014).

[17] T. Blasingame, *Properties of homogeneous reservoirs, naturally fractured reservoirs, and hydraulically fractured reservoirs from decline curve analysis,* SPE , 279 (1986).

[18] B. Singhal, *Applied hydrogeology of fractured rocks,* Springer Science + Business Media , 13 (2010).

[19] Y. Jia, *Flow modeling of well test analysis for porous-vuggy carbonate reservoirs,* State Key Laboratory of Oil Gas Reservoir Geology and Exploitation , 253 (2012).

[20] B. Dershowitz, *Fracture aperture correlations,* Rock Mechanics Geomechanics Symposium (2012).

[21] R. Nelson, *Geologic analysis of naturally fractured reservoirs,* Gulf Professional Publishing **2** (2001).

[22] B. Clausmann, *Integrated subsurface review of the zechstein reservoir in the northeast netherlands,* Vermillion Energy, internship report (2012).

[23] M. Fetkovich, *Decline curve analysis using type curves - case histories,* SPE (1987).

[24] F. Kuchuk, *Fractured-reservoir modeling and interpretation,* SPE (2015).